Neurobiology of Disease

The Amyloid Precursor Protein Modulates the Position and Length of the Axon Initial Segment

Fulin Ma,[1,3] Himanshu Akolkar,[1] Jianquan Xu,[2] Yang Liu,[2] Dina Popova,[4] Jiaan Xie,[2] Mark M. Youssef,[5] Ryad Benosman,[6] Ronald P. Hart,[4,5] and Karl Herrup[1,2]

[1]Department of Neurobiology, University of Pittsburgh School of Medicine, Pittsburgh, PA 15261, [2]Departments of Medicine and Bioengineering, University of Pittsburgh School of Medicine, Pittsburgh, PA 15261, [3]Division of Life Science, Hong Kong University of Science and Technology, Clear Water Bay, Kowloon, Hong Kong, [4]Human Genetics Institute, Rutgers University, Piscataway, NJ 08854, [5]Department of Cell Biology and Neuroscience, Rutgers University, Piscataway, NJ 08854, and [6]Robotics Institute, Carnegie Mellon University, Pittsburgh, PA 15213

The amyloid precursor protein (APP) is linked to the genetics and pathogenesis of Alzheimer's disease (AD). It is the parent protein of the β-amyloid (Aβ) peptide, the main constituent of the amyloid plaques found in an AD brain. The pathways from APP to Aβ are intensively studied, yet the normal functions of APP itself have generated less interest. We report here that glutamate stimulation of neuronal activity leads to a rapid increase in *App* gene expression. In mouse and human neurons, elevated APP protein changes the structure of the axon initial segment (AIS) where action potentials are initiated. The AIS is shortened in length and shifts away from the cell body. The GCaMP8f Ca^{2+} reporter confirms the predicted decrease in neuronal activity. NMDA antagonists or knockdown of *App* block the glutamate effects. The actions of APP on the AIS are cell-autonomous; exogenous Aβ, either fibrillar or oligomeric, has no effect. In culture, APP_{Swe} (a familial AD mutation) induces larger AIS changes than wild type APP. Ankyrin G and βIV-spectrin, scaffolding proteins of the AIS, both physically associate with APP, more so in AD brains. Finally, in humans with sporadic AD or in the R1.40 AD mouse model, both females and males, neurons have elevated levels of APP protein that invade the AIS. *In vivo* as *in vitro*, this increased APP is associated with a significant shortening of the AIS. The findings outline a new role for the APP and encourage a reconsideration of its relationship to AD.

Key words: **Alzheimer's disease; action potential; Aβ; excitotoxicity; Ankyrin G; βIV-spectrin**

Significance Statement

While the amyloid precursor protein (APP) has long been associated with Alzheimer's disease (AD), the normal functions of the full-length Type I membrane protein have been largely unexplored. We report here that the levels of APP protein increase with neuronal activity. *In vivo* and *in vitro*, modest amounts of excess APP alter the properties of the axon initial segment. The β-amyloid peptide derived from APP is without effect. Consistent with the observed changes in the axon initial segment which would be expected to decrease action potential firing, we show that APP expression depresses neuronal activity. In mouse AD models and human sporadic AD, APP physically associates with the scaffolding proteins of the axon initial segment, suggesting a relationship with AD dementia.

Introduction

Most models of Alzheimer's disease (AD) pathogenesis focus on a small peptide known as β-amyloid (Aβ). Aβ is the main constituent of the plaques found in the AD brain and is derived by proteolytic cleavage of a large Type I membrane protein known as the amyloid precursor protein (APP) (Goldgaber et al., 1987; Kang et al., 1987; Tanzi et al., 1987). The link to AD is compelling as mutations near the cleavage sites on APP that release Aβ have been identified as autosomal dominant AD disease genes. Further, as APP is located on human chromosome 21, individuals with Down syndrome make supranormal amounts of APP and show early-onset clinical and pathologic signs of Alzheimer's-like dementia (Ness et al., 2012).

Received Jan. 23, 2022; revised Jan. 23, 2023; accepted Jan. 24, 2023.

Author contributions: F.M., R.P.H., and K.H. designed research; F.M., H.A., J. Xu, D.P., J. Xie, and M.M.Y. performed research; F.M., H.A., J. Xu, Y.L., J. Xie, M.M.Y., R.B., R.P.H., and K.H. analyzed data; F.M. wrote the first draft of the paper; F.M., H.A., J. Xu, Y.L., D.P., J. Xie, R.B., R.P.H., and K.H. edited the paper; F.M. wrote the paper; H.A. and Y.L. contributed unpublished reagents/analytic tools.

This work was supported by Hong Kong University of Science and Technology Grant R9321; University of Pittsburgh School of Medicine start-up support and a Pitt Momentum award to K.H. and R.B.; and National Institutes of Health Grants R01 CA254112 to Y.L. and 5U10 AA008401 to R.P.H. We thank the Neuropathology Core of the Alzheimer's Disease Research Center at University of Pittsburgh for providing human samples. The Alzheimer's Disease Research Center is supported by National Institute on Aging Grants P30 AG066468 and P50 AG005133.

The authors declare no competing financial interests.

Correspondence should be addressed to Karl Herrup at herrup@pitt.edu.

https://doi.org/10.1523/JNEUROSCI.0172-22.2023

Yet while much is known about the Aβ peptide, the normal function(s) of the full-length precursor protein remain little studied. APP is an evolutionarily ancient protein with analogs found, even in invertebrates such as nematodes and fruit flies (Zheng and Koo, 2006). It is expressed in tissues throughout the body (Uhlen et al., 2015), including brain. Its mRNA is found in astrocytes and neurons, but it is equally abundant in oligodendrocytes and endothelial cells (Zhang et al., 2014). APP expression begins at the pre-implantation stage of development (Fisher et al., 1991), and several developmental roles have been suggested. For example, during CNS development, mis-regulated expression of APP leads to defective cortical neuron migration (Young-Pearse et al., 2007). APP is found at the growth cone and mediates axon guidance (Kibbey et al., 1993; Rama et al., 2012; Wang et al., 2017). As neurons begin maturation, APP helps guide synapse formation (Priller et al., 2006; Klevanski et al., 2015), and promote dendritic spine formation (Lee et al., 2010). In the mature organism, APP mediates many fundamental cellular processes (Muller et al., 2017). The large extracellular domain of APP, known as secreted APP, has a variety of functions (Mattson et al., 1993; Furukawa et al., 1996; Mockett et al., 2017). The intracellular portion of APP (known as the APP intracellular domain), similar to the homologous portion of the Notch protein, translocates to the nucleus, although its function there is not well understood (Cao and Sudhof, 2001; Gao and Pimplikar, 2001). Finally, APP is a damage response protein. Multiple studies have shown that, in response to stress, the levels of APP in neurons increase, particularly at a site of axonal injury (Gentleman et al., 1993; Sherriff et al., 1994; Miyai et al., 2021; Muñoz et al., 2021).

We report here a new biological function for APP. We find that APP is a dynamic modulator of the axon initial segment (AIS), a specialized cellular compartment found at the junction between the neuronal soma and axon. The AIS is the site of action potential initiation as well as a barrier that helps maintain neuronal polarity (Colbert and Johnston, 1996; Jenkins and Bennett, 2001; Hedstrom et al., 2008; Kole et al., 2008; Ogawa and Rasband, 2008; Nelson and Jenkins, 2017; Huang and Rasband, 2018). Through changes in its length and cellular location, the AIS modulates firing probability and thus can fine-tune neuronal activity (Song et al., 2009; Grubb and Burrone, 2010a; Kuba et al., 2014). We show here that, after an excitotoxic challenge, APP levels rise in the AIS, concurrent with changes in its length and cellular location. We further show that APP overexpression alone is sufficient to alter AIS position and length. Finally, the AIS changes are observed in APP overexpressing transgenic mice, as well as in human sporadic AD, yet are independent of the presence of Aβ plaques. These findings offer a possible new connection between the symptoms of AD and the normal function of APP.

Materials and Methods

Human samples. Postmortem brain tissue was obtained from the National Institutes of Health NeuroBioBank at the University of Maryland, Baltimore, MD, the Human Brain and Spinal Fluid Resource Center, and the Mount Sinai/James J. Peters VA Medical Center, National Institutes of Health Brain and Tissue Repository, with approvals from Tissue Access Committee of NeuroBioBank. Subjects with AD and age-matched unaffected controls (UCs) were requested; any cases with >10 h postmortem interval were excluded. Both UC (Braak Stage 0-II) and AD (Braak Stage V-VI) female and male samples between the ages of 76 and 82 were used in this study. All tissues were from left frontal cortex (Brodmann area 9) that had been frozen without prior fixation and stored at −80°C. Tissues were cryosectioned at 10 μm and stored at −80°C until use.

Animals. A colony of R1.40 transgenic mice (B6.129-Tg (APPSw) 40Btla/Mmjax) was established from mice originally purchased from The Jackson Laboratory. The R1.40 colony is maintained on the C57BL/6J background. Wild type littermates served as controls. Both genders of the mice were used in this study. Two females and 2 males of each genotype were examined. Initial experiments were conducted in Hong Kong. These were conducted with under regulations established by the Government of Hong Kong SAR and were approved by the Animal Ethics Committee of the Hong Kong University of Science and Technology. Colonies were maintained and bred in the Animal and Plant Care Facility at Hong Kong University of Science and Technology, and all animal procedures complied with university guidelines and the Government of Hong Kong Department of Health.

Additional animals used in this study were derived from stock maintained and bred in Pittsburgh in the facility maintained by the Division of Laboratory Animal Resources, University of Pittsburgh, School of Medicine. For animals used in Pittsburgh, all protocols were approved by the Institutional Animal Care and Use Committee. Animals were treated in compliance with the Institute for Laboratory Animal Research of the National Academy of Sciences' *Guide for the care and use of laboratory animals*.

Genotyping for the R1.40 transgene locus was done with the recommended PCR primers using the PCR Ready Mix kit (E3004; Sigma-Aldrich). The sequences of the genotyping primers were as follows: R1.40 transgene forward: 5′-CTT CAC TCG TTC TCA TTC TCT TCC A-3′; R1.40 transgene reverse: 5′-GCG TTT TTA TCC GCA TTT CGT TTT T-3′; internal control forward: 5′-CAA ATG TTG CTT GTC TGG TG-3′; internal control reverse: 5′-GTC AGT CGA GTG CAC AGT TT-3′.

Primary culture. The culture surface of each well was coated with poly-L-lysine (0.5 mg/ml, diluted in boric acid buffer, Sigma). Wild type E16.5 C57BL/6J embryos were harvested from gravid females. After decapitation, their cerebral cortices were isolated and stored at 4°C in PBS with 1 mg/ml glucose. Cortices were cut into small pieces using forceps and treated with 0.25% trypsin-EDTA (Sigma) for 10 min at 37°C. The tissue was then washed in 10% FBS in DMEM to inactivate the trypsin, then washed in Neurobasal medium (Invitrogen), and triturated to produce a single-cell suspension. Cells were plated onto poly-L-lysine-coated coverslips in 24-well plates at a density of 48,000 cells/well. The medium to maintain the neurons was Neurobasal medium supplemented with 2% B27 (Invitrogen), 1% Glutamax (Invitrogen), and 10,000 U/ml penicillin/streptomycin (Invitrogen). Cultures were maintained at 37°C in a humidified atmosphere of 5% CO_2. Every 5 d, the culture medium was refreshed by replacing half of the old medium.

Human neuron induction. An iPS line was prepared from a healthy, 23-year-old female subject of European ancestry. Cryopreserved lymphocytes were reprogrammed to iPSC using Sendai-viral-expressed transcription factors (Oct3/4, Sox2, Klf4, and c-Myc; CytotuneTM-iPS Reprogramming Kit, Fisher Scientific) by RUCDR Infinite Biologics (now Sampled). Pluripotent cells were selected by colony morphology, alkaline phosphatase positivity, and immunocytochemical expression of Oct4 and TRA-1-60. The pluripotency of resulting iPSC was subsequently confirmed by colony morphology and immunocytochemistry for Oct4 and Tra-1-60 markers (Popova et al., 2023). To generate glutamatergic neurons, iPS cultures were infected with lentiviruses carrying the neuronal transcription factor Neurogenin2 (*Ngn2*) and a reverse tetracycline-controlled transactivator, in mTeSR medium (Stem Cell Technologies) with 1.5 μM ROCK inhibitor (Y27632, Tocris), as described previously (Zhang et al., 2013). The following day, the medium was replaced with Neurobasal containing B27 supplement (Fisher Scientific), GlutaMAX, 2 μg/ml doxycycline, and 5 μM ROCK inhibitor. Twenty-four hours following induction, transduced cells were selected with 1 μg/ml puromycin with doxycycline. Four days later, on day 5, cells were dissociated with Accutase (Stem Cell Technologies) and replated onto a monolayer of primary mouse glial cells on glass coverslips. The medium was transitioned to Neurobasal Plus medium containing B27 Plus supplement and CultureOne supplement (Fisher Scientific), with GlutaMAX and 200 mM ascorbic acid and replenished every 3-4 d. To inhibit glial overgrowth, 2 μM cytosine arabinoside was used as needed. Treatment and morphologic analyses were conducted 4-5 weeks following initial induction with doxycycline.

Plasmids. A construct encoding human APP bearing the Swedish mutation (APP_{Swe}) was kindly provided by Amy Fu of Hong Kong

University of Science and Technology. The APP-GFP construct with human APP and C-terminal GFP tag was provided by Hei-man Chow at Hong Kong University of Science and Technology. APP shRNA (pENTR APP shRNA 2) was acquired from Addgene (Plasmid #30135) and recloned into a lentiviral plasmid. FUGW-APP_{Swe} virus (Addgene 190804) and synapsin-driven GCaMP8f lentivirus plasmid were provided by Ronald Hart.

Transfection. Transfection was performed using Lipofectamine LTX with plus reagent kit (Fisher Scientific A12621). Each plasmid was diluted to 50 ng/µl in Opti-MEM medium and incubated for 5 min at room temperature. Then 2 µl of lipofectamine-LTX was added to a separate 50 µl of Opti-MEM. The two portions of Opti-MEM were mixed for a final volume of 100 µl and incubated for 20 min at room temperature before adding to the neurons. After 5 h of incubation, the medium was changed back to conditioned medium. Neurons were cultured *in vitro* for 7 d (DIV7) in a 5% CO_2 atmosphere at a density of 24,000 cells per well of a 24-well plate with medium half-replaced once with fresh NeuroBasal medium at DIV5. The medium was changed from NeuroBasal complete to NeuroBasal without antibiotics at a final volume of 400 µl. The conditioned medium was collected and stored at 4°C after which the 100 µl mixture of DNA/lipofectamine-LTX was then added without disruption into one well of the 24-well plates. The neurons were incubated for 4 h and then changed back to their previously conditioned medium after it had been prewarmed. The neurons were cultured at 37°C in a 5% CO_2 atmosphere for 2 more days before fixation or initiation of other treatments.

Tissue processing. R1.40 mice and littermate controls at 18 months of age were used for histologic analysis. Animals were anesthetized by a 1:1 mixture of 10 mg/ml ketamine (Covetrus) and 2 mg/ml xylazine (Covetrus) at a dose of 0.02 ml/g. The mice were then perfused with 2 ml 0.9% saline at a flow rate of 10 ml/min. The brains were dissected free of the skull, and the cortex was bisected on the midline. The left hemisphere was frozen on dry ice and stored at −80°C until used for immunoblotting. To prepare tissue for histology, the right hemisphere was postfixed by immersion in 4% paraformaldehyde for 24 h. After postfixation, the brains were cryoprotected by incubation in 30% sucrose in PBS for 24 h. The brains were then embedded into OCT blocks for cryosectioning at 10 µm, in either the coronal or sagittal plane. Sections were stored in −80°C until processed for immunohistochemistry or immunofluorescence.

Immunochemistry. For tissue culture cells, after fixation and washing with PBS, cells were permeabilized with 0.5% Triton X-100 in PBS (PBST). Cells were blocked for 1 h at room temperature with PBST containing 5% donkey serum then incubated overnight at 4°C with primary antibody in PBST at the dilutions listed in Table 1. The next day, cells were washed in PBS and incubated with secondary antibody diluted at 1:500 in PBST for 1 h at room temperature, followed by staining with DAPI for 5 min. The coverslips were then mounted in Hydromount and viewed on a fluorescence microscope (Olympus DP80) or on a confocal microscope (Nikon Eclipse Ti2).

For both human and mouse brain tissue, cryosections were immersed in citrate buffer (pH 6.0) and heated at 95°C for 10 min for antigen retrieval. After cooling and rinsing, the sections were incubated in 10% donkey serum at room temperature for 1 h to reduce nonspecific antibody binding followed by overnight incubation at 4°C with the primary antibody. The primary antibodies used, along with their sources, are listed in Table 1. After rinsing, the sections were incubated in AlexaFluor-conjugated secondary antibody for 1 h at room temperature. Cell nuclei were counterstained with DAPI. For each biological repeat, at least three sections were processed using the above-mentioned method and three ROIs per section were imaged for quantification. The ROIs were chosen by first identifying the region where the measurements were to be taken at low power using only the DAPI channel. Once selected, a higher magnification was chosen at random from the low-power field, an image captured with the camera in all fluorescent channels, and the resulting image used for the quantifications described. Fluorescent imaging was done on a Nikon Eclipse Ti2 Confocal microscope with a 60× (1.4 Numerical Aperture) oil objective lens and A1R (Andor, 512 µm × 512 µm) camera, X-Cite 120 LED illumination system, and a DAPI (400-418 nm), FITC (450-490 nm), TRITC (554-570 nM), and Cy5 (640-670 nm) filter sets controlled by NIS-Elements AR software.

Table 1. Antibodies

Target name	Manufacturer	Catalog #	Dilution used
MAP2	Abcam	ab5392	1:2500
6E10	Covance	SIG-39320	1:1000
APP-N′	Abcam	ab15272	1:400
APP-N′ (KO validated)	Abcam	ab133509	1:400
AnkG	Millipore	MABN466	1:500
βIV spectrin	Dr. Mathew Rasband	NA	1:250

RNA isolation and qPCR. DIV14 neurons treated with 1 µM glutamate for the times indicated in the text then harvested using the QIAGEN RNeasy Mini kit (QIAGEN, 74104) according to the manufacturer's instructions. For each sample, an equal amount (500 ng) of RNA was reverse transcribed to cDNA using iScript reverse-transcription kit (Bio-Rad, 1708841). qRT-PCR (45 cycles: LightCycler480 software) was performed using fast SYBR Green Master Mix (Bio-Rad 1725122). GAPDH served as a loading control. The sequence of *App* primers are as follows: forward, ACTCTGTGCCAGCCAATACC; reverse, GAACCTGGTCGAG TGGTCAG.

Stochastic optical reconstruction microscopy (STORM). For STORM imaging, cells were incubated with the primary antibody at 4°C overnight, and then with Alexa647-conjugated and CF568-conjugated goat-anti-rabbit/mouse secondary antibody for 2 h at room temperature. STORM imaging was done on a custom-built STORM imaging system in the Liu laboratory based on an Olympus IX71 inverted microscope frame with a 100×, NA = 1.4 oil immersion objective (UPLSAPO 100XO, Olympus), as described previously (Xu et al., 2018). For two-color STORM imaging, 30,000 frames were acquired at an exposure time of 20 ms per frame for each color (642 and 561 nm). Online drift correction was independently performed every 200 frames (~4 s) with fluorescent beads (Fisher Scientific, F8803) as fiduciary markers (excited with 488 nm laser) throughout the image acquisition process, based on our established method (Ma et al., 2017). In contrast to the periodic appearance of βIV-spectrin in super-resolution images of the AIS (Xu et al., 2013), the pattern we observed using our AnkG antibody is more uniform. This is to be expected as the antibody was raised against the C-terminal amino acids of the ankyrin G protein. This portion of AnkG is explicitly not periodic (Leterrier et al., 2015).

Image analysis and fluorescence intensity quantification. Fiji software and MATLAB were used to quantify the cellular and AIS fluorescence intensity. For cellular fluorescence intensity, freehand line tool was used to select the outline of a cell body with MAP2 staining as counterstained ROI. An average of three background regions with the same area as a given cell body stain was used as control for background staining and subtracted from each image. Raw Integrated Density was used as measurement for the cellular intensity.

Western blots. Cultured cells were harvested and homogenized in ice-cold RIPA buffer (EMD Millipore) with 1× PhosSTOP phosphatase inhibitor mixture (Roche Applied Science) and 1× complete protease inhibitor cocktail (Roche Applied Science). The homogenate was then centrifuged at 4°C for 20 min at 15,000 rpm. The supernatant containing protein was collected. Human brain samples (200 mg from Brodmann area 9 [BA9]) were acquired from Mount Sinai and the NIH NeuroBioBank. A fraction of each specimen was homogenized using the protocol of Nelson et al. (2020). Briefly, the tissue was homogenized in buffer containing 8 M urea, 5% SDS, and 5 mM N-ethylmaleimide in a 1.5 ml microcentrifuge tube then hand-dounced in 10 volumes/weight of 65°C homogenization buffer. The homogenate was next incubated at 65°C for 20 min. After the incubation, the sample was mixed 1:1 with 5× PAGE buffer (5% (w/v) SDS, 25% (w/v) sucrose, 50 mM Tris, pH 8, 5 mM EDTA, bromophenol blue). The lysates were stored at −80°C until use. Protein concentration was determined using the Bradford assay (Bio-Rad). A total of 10 µg protein was then separated by SDS-PAGE and transferred to Immuno-Blot PVDF membranes (Bio-Rad). Membranes were incubated in 5% nonfat milk for 1 h at room temperature to block nonspecific binding. Primary antibodies were applied at room temperature overnight.

After rinsing 3 times with TBST, membranes were incubated with secondary antibodies for 1 h at room temperature. Signals were visualized with SuperSignal West Pico, Dura, or Femto chemiluminescent substrate (Fisher Scientific). For the 480 kDa AnkG immunoblotting gel, a high molecular weight protein standard was used (Fisher Scientific LC5699). For all other gels, the protein standard used was a normal wide range from 5 to 250 kDa, Precision Plus Protein Dual Color Standards (Bio-Rad 1610374).

Coimmunoprecipitation. Wild type and R1.40 brains were homogenized in a Dounce homogenizer. The lysates were then incubated in coimmunoprecipitation buffer (20 mM Tris HCl, pH 8.0, 137 mM NaCl, 1% Nonidet P-40 (v/v) and 2 mM EDTA) on ice for 30 min. The brain lysates were incubated with primary antibody and protein G magnetic beads overnight at 4°C with moderate shaking. Then the beads were washed with coimmunoprecipitation buffer 3 times and eluted with 1× SDS-PAGE loading buffer. The eluted proteins were then run on SDS/polyacrylamide gels and subjected to Western blotting.

Aβ fibril and oligomer preparation. Beta amyloid ($A\beta_{1\text{-}42}$) aggregation kit was purchased from rPeptide (A-1170-2). To produce fibrillar Aβ, the Aβ powder was dissolved in NeuroBasal medium to a final concentration of 220 μM, followed by incubation for 5 d at 37°C. To prepare Aβ oligomers, 22.2 μl DMSO was added to 0.5 mg of HFIP-treated $A\beta_{1\text{-}42}$ (A-1163-1) to a final concentration of 5 mM. The Aβ and DMSO mixture was then vortexed for 30 s to make sure all the Aβ powder was dissolved in DMSO followed by a short centrifugation. The solution was sonicated for 10 min in a bath sonicator followed by the addition of 1087 μl cold 4°C phenol-red-free F-12 medium to achieve a final concentration of 100 μM. The Aβ solution was then vortexed for 15 s and incubated at 4°C for 24 h. Afterward, Aβ was centrifuged at 14,000 × *g* for 10 min at room temperature. The supernatant was then collected for use.

Statistical analysis. Data are expressed as mean ± SEM for each group. The statistical significance of changes in different groups was evaluated by unpaired Student's *t* test using GraphPad Prism software. *p* values <0.05 were considered to be significant.

Results

Activity increases APP levels and causes AIS length and position to change

APP is recognized as a stress response protein. Following oxidative stress, excitotoxicity, or exposure to free radicals, APP protein levels increase (Frederikse et al., 1996; Masliah et al., 1997; White et al., 1999). This is relevant to the situation in AD as excitotoxicity is cited as an important risk factor (Greenamyre and Young, 1989). Indeed, blunting the effects of excitotoxicity is the theoretical mechanism of action of the FDA-approved AD drug, memantine (Johnson and Kotermanski, 2006). To test this association of APP with excitotoxicity *in vitro*, we used E16.5 mouse cortical neurons cultured for DIV14 and exposed them to a relatively low concentration of glutamate (1 μM). We found that, in treated but not untreated cells, the intensity of neuronal APP immunostaining increased noticeably 24 h following glutamate addition, although MAP2 immunostaining revealed no major structural changes in dendritic integrity (Fig. 1*A–D*). The increased APP fluorescent signal was obvious in the cell body as well as in the dendrites and was blocked by preincubating the neurons with 20 μM dCPP, a selective NMDAR antagonist (Monnet et al., 1995; Costa et al., 2009).

While the quantitative increase in staining was evident throughout the cell, we also observed a qualitative change in the axon and AIS. We identified the axonal process and the location of the AIS by immunostaining with the scaffolding protein, ankyrin G (AnkG, red signal, Fig. 1*A–D*, white arrows). In untreated cells, the axon had low, but detectable, amounts of APP immunoreactivity (Fig. 1*A*, green signal). After a 24 h treatment with 1 μM glutamate, however, APP infiltrated the axon hillock and the AIS (Fig. 1*C*). Using ImageJ software, we found that the average APP fluorescent signal intensity increased more than twofold in the AIS of treated neurons (Fig. 1*E*). This expansion of the domain of APP staining was found in virtually every neuron in our cultures. Although the initial assays were performed after 24 h, the APP response to the glutamate challenge was far more rapid. We exposed DIV14 neuronal cultures to 1 μM glutamate, harvested the cells after varying lengths of time, and performed qPCR on the cell lysates. After 30 min of stimulus, the level of *App* mRNA started to rise and within 1 h was increased threefold to fivefold (Fig. 1*J*). This is consistent with the documented role of APP as a stress response protein.

In addition to the increased level of APP in glutamate-treated neurons, the properties of the AIS, as revealed by the pattern of Ankyrin G staining, also changed. Its length was significantly reduced, and the distance between the cell body and the proximal end of the AIS was significantly increased (Fig. 1*F*,*G*). These changes were mediated by glutamate directly, acting through the NMDAR. A 30 min pretreatment of the cultures with dCPP completely blocked the AIS changes as well as the increase in APP protein (Fig. 1*H*,*I*). One plausible interpretation of these findings is that the activity caused by glutamate led to an increase in APP and that it was the increased APP that led to the changes in the AIS. The AIS changes in turn would be expected to increase the threshold for initiating an action potential (Grubb and Burrone, 2010a; Evans et al., 2013; Muir and Kittler, 2014).

Overexpression of APP is sufficient to change the AIS configuration

To test the idea that APP regulates the configuration of the AIS, we asked whether, in the absence of a glutamate stimulus, increased APP alone would be sufficient to produce similar effects. We cotransfected APP-encoding and GFP-encoding plasmids into DIV7 cultured neurons. Control cultures were transfected with only a GFP plasmid. Two days later, the cells were fixed and immunostained for MAP2 and either βIV spectrin or AnkG (Fig. 2*A–C*). Transfected neurons had elevated APP that infiltrated all processes, including the axon. Consistently, in APP-expressing neurons, the length of the AIS was reduced by almost one-half compared with control. The distance from the cell body to the proximal end of the AIS also increased (Fig. 2*B*). Thus, APP overexpression alone, in the absence of glutamate stimulation, is sufficient to cause the AIS to shift away from the cell body and reduce in length.

The AIS in AD: *in vitro* data

That APP overexpression can result in significant changes in the AIS raises the question of whether the elevated levels of APP that are found in AD have similar effects and thus possibly contribute to the symptoms of dementia. We tested this idea first by comparing the properties of the AIS in neurons transfected with either the WT human *APP* (*hAPP*) or the well-characterized Swedish variant, K595N/M596L ($hAPP_{Swe}$), an autosomal dominant disease gene that causes early-onset AD. We found that cells transfected with $hAPP_{Swe}$ underwent a shrinkage of the AIS that was nearly 50% greater than that found with wild type (WT) hAPP (Fig. 2*A–C*). Neither WT hAPP nor $hAPP_{Swe}$ overexpression caused visible damage to the transfected neurons. At 2 d after transfection, the appearance of the MAP2-immunostained dendritic structure was not notably different from neurons expressing only the control GFP vector.

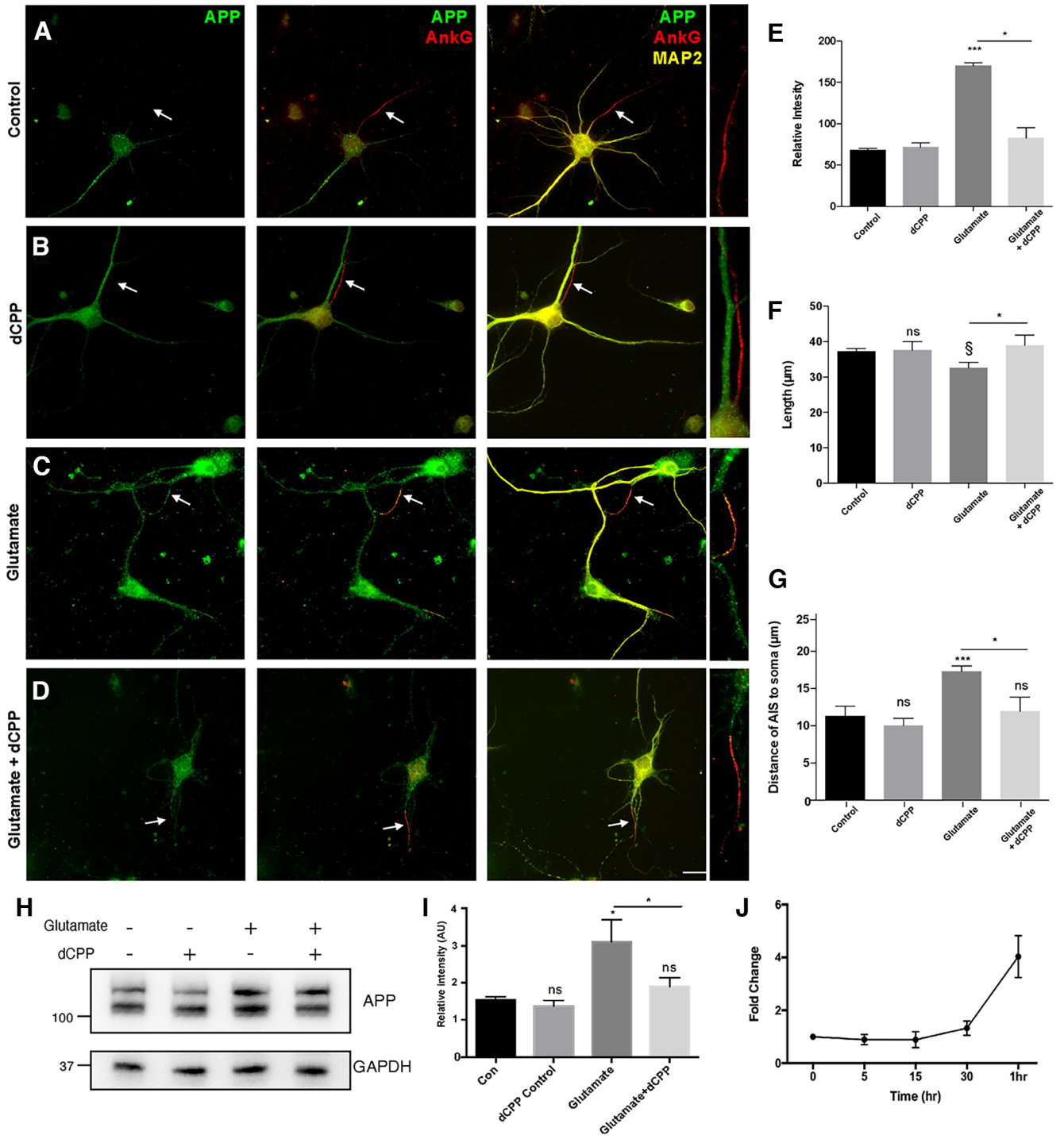

Figure 1. Glutamate stimulation affects cellular APP levels and the length and location of the AIS. ***A–D***, Immunofluorescent staining of DIV14 primary cultured neurons after a 24 h treatment with 1 μM glutamate, with or without the protection of dCPP. Right insets, Axon designated by the white arrow (***A***) untreated control; (***B***) 20 μM dCPP: (***C***) 1 μM glutamate; and (***D***) 20 μM dCPP added 30 min before 1 μM glutamate. Green represents APP. Red represents ankyrin G (AnkG). Yellow represents MAP2. ***E***, Intensity of APP immunofluorescent signal in the AIS measured using Fiji software. ***F***, Length of the AIS after the indicated treatments. ***G***, Distance from the cell soma to the proximal end of the AIS. ***H***, Western blot of APP protein after treatments. ***I***, Quantification of band intensities shown in ***H***. ***J***, RT-PCR measurements of *APP* mRNA at various times after treatment with 1 μM glutamate. Data are mean ± SEM. Symbols over individual bars represent significance of difference from control. *$p < 0.05$; ***$p < 0.001$; §$p < 0.05$ ANOVA. $n = 4$ independent cultures. At least 15 neurons were quantified in each individual culture. Scale bar, 10 μm.

We were concerned that the levels of APP protein after transfection might be artificially high, so much so that they would create a cellular state that did not reflect normal physiological conditions. We therefore cultured cortical neurons from brains of the R1.40 mouse AD model, whose $hAPP_{Swe}$ transgene is expressed at only 2-3 times the levels of the endogenous mouse *App* gene (Lamb et al., 1993, 1997). This is close to the increase in mouse *App* expression observed following a glutamate challenge (Fig. 1*J*). We found that the response of the AIS, even with this more modest increase in APP expression, was still significant. In R1.40 neurons, axonal APP immunostaining invaded the axon hillock as well as the AIS, and the length of the AIS was reduced compared with neurons cultured from WT animals of the same litter (Fig. 2*D*,*E*). Compared with the APP_{Swe}-transfected neurons,

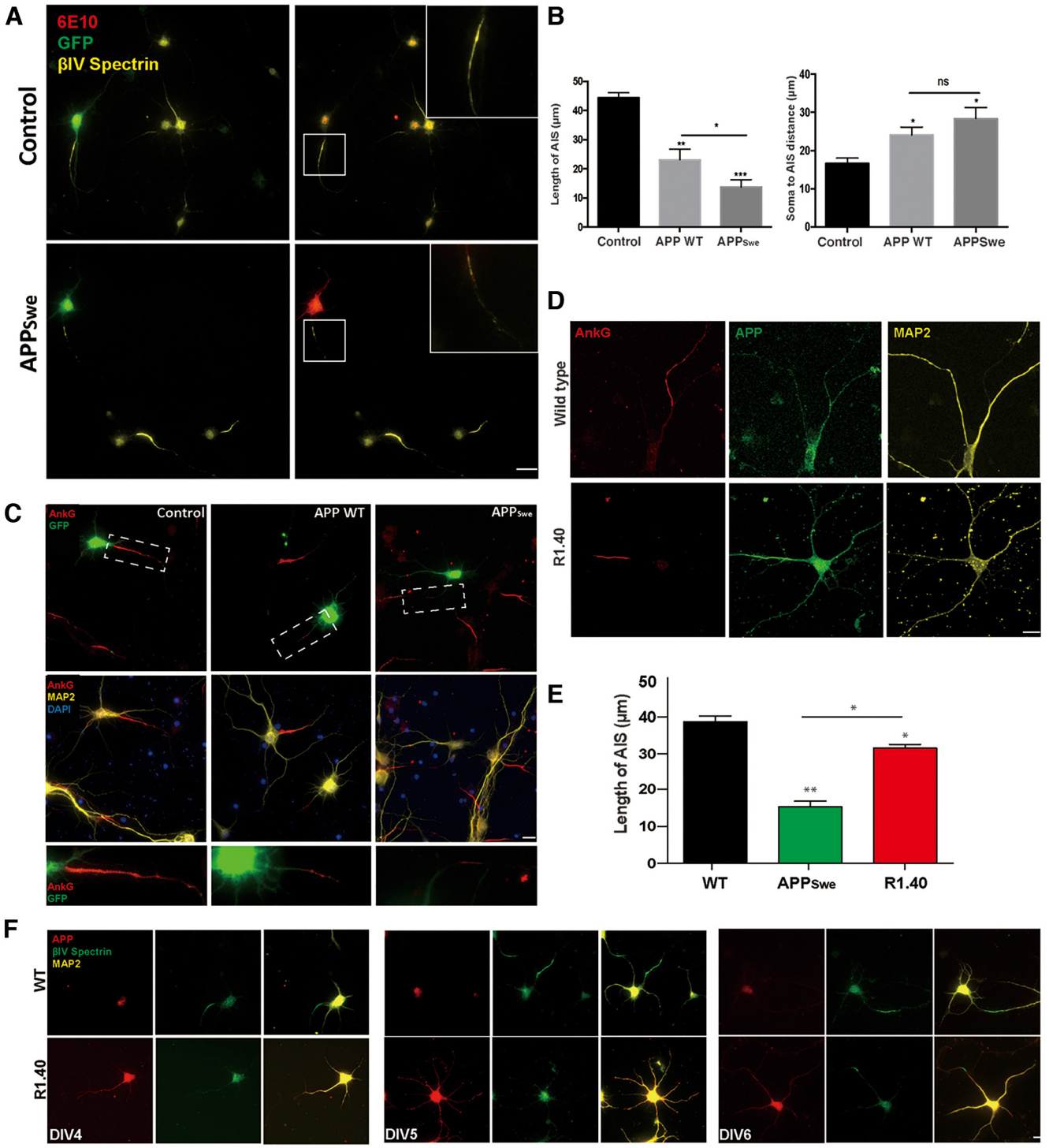

Figure 2. APP overexpression induces AIS changes. ***A***, Cultured cortical neurons, cotransfected on DIV7 with APP_{Swe} and GFP plasmids, were immunostained with antibodies against βIV spectrin (yellow) to mark the AIS and 6E10 (red) to show the location of APP. Cultures were fixed 2 d after transfection. Scale bar, 10 μm. ***B***, Quantification of the AIS length (left) and distance to soma (right) in transfected neurons. ***C***, Cultured cortical neurons were cotransfected on DIV7 with GFP as well as with either WT APP or APP_{Swe} plasmids. Cultures were fixed and immunostained for AnkG (red) and MAP2 (yellow) 2 d after transfection. Scale bar, 10 μm. Data are mean ± SEM. $*p < 0.05$; $**p < 0.001$; one-way ANOVA. $n = 4$. ***D***, Confocal image of the AIS immunolabeled with AnkG (red), N-terminal APP antibody (N′APP. green), and MAP2 (yellow). Cells were from DIV14 cortical neuron cultures from WT (top row) or R1.40 (bottom row) cultures. Scale bar, 10 μm. ***E***, Quantification of the AIS lengths in cultures of APP_{Swe} transfected or R1.40 transgenic neurons. Data are mean ± SEM. Symbols over individual bars represent significance of difference from WT. $*p < 0.05$; $**p < 0.001$; one-way ANOVA. $n = 4$. ***F***, Immunolabeling of APP (red) in the developing axon using βIV spectrin (green) to label the AIS. MAP2 (yellow) was used as a dendritic marker. Scale bar, 5 μm.

the reduction of the length of the R1.40 AIS was less dramatic (Fig. 2*E*). This suggests that the APP-driven shortening of the AIS is both dose- and genotype-dependent. Intriguingly, the APP effect is seen even during neuronal maturation. We used βIV spectrin to track the appearance of the AIS as a function of time in culture. In WT neurons, the AIS begins to form in the growing axons after DIV4. In R1.40 neurons, by contrast, the AIS does not appear until DIV6 (Fig. 2*F*).

To obtain a more fine-grained picture of the interplay of APP with the components of the AIS, we used STORM. The resulting high-resolution images showed that, in WT mouse cultures, endogenous APP (stained with an APP N-terminal antibody) gave a weak signal in the AIS but was clearly visible in the cell body (Fig. 3*A*). In R1.40 neurons, however, APP staining was stronger and could be found entering the axon and the region of the AIS. The impression gained when comparing this pattern with that of the AnkG scaffold protein was that APP was "pushing" the AIS away from the cell body. Quantification of the relative signal intensity of the two antibodies was consistent with this idea (Fig. 3*B*).

We next asked whether the AIS scaffold proteins physically interacted with APP. We prepared lysates from frozen brain samples of UC and AD patients (Brodmann area 9). We performed immunoprecipitations with AnkG or βIV spectrin antibodies, or with a KO-validated APP N-terminus antibody (APP-N′), and then probed Western blots of the precipitates with an AnkG antibody (Fig. 3*C*). Both AnkG and βIV spectrin antibodies pulled down the expected three species of AnkG (Fig. 3*C*, top and bottom gel, lanes 2 and 3). Immunoprecipitation of Alzheimer's brain lysates sample using the 6E10 and APP antibody also pulled down AnkG (Fig. 3*C*, bottom gel lane 4). A similar result was found with lysates from UC tissue, but the strength of the AnkG band was considerably reduced (Fig. 3*C*, top gel, lane 4). To further explore the details of this interaction, we quantified the amounts of AnkG brought down by APP immunoprecipitation, normalizing the results to the amount brought down by AnkG itself. We found that the APP pulled down nearly twice as much AnkG from the AD brain as from UC tissue. This was true for both the 480 and 270 kDa AnkG (Fig. 3*D*). Curiously, while the 190 AnkG isoform was present in the APP immunoprecipitates, its levels were largely unchanged between the AD and UC samples. Thus, in human AD brain lysates, the physical interaction of AnkG and APP is more extensive than in control lysates. The same pattern of association was found with lysates from WT and R1.40 mouse brains (data not shown). Together, these results demonstrate that APP, a membrane protein implicated in AD, is colocalized and physically associated with an important scaffolding protein of the AIS.

The data thus far show that upregulation of APP, induced either genetically or by a glutamate stimulus, is sufficient to change the length and location of the AIS. We next asked what were the effects of reducing the level of APP on the structure of the AIS. We cotransfected cultured cortical neurons with a plasmid encoding APP shRNA plus a GFP plasmid (to identify transfected cells) 48 h before treating them with 1 μM glutamate. We monitored the effectiveness of the shRNA knockdown in two ways. First, we measured the intensity of APP immunostaining in transfected (GFP-positive) compared with nontransfected cells and found it to be reduced by >80% (Fig. 3*E*,*F*). Second, we infected sister cultures with shAPP or scrambled control, lysed the cells, and ran Western blots for total APP protein (Fig. 3*I*). The intensity of the APP band was reduced relative to the loading control (Fig. 3*I*).

To see the effect of APP knockdown, we immunostained the AIS with AnkG. In control cells (transfected with a scrambled shRNA), after exposure to 1 μM glutamate, the length of the AIS was reduced and its distance from cell soma increased (Fig. 3*E*,*G*,*H*) just as was seen in nontransfected cells (not shown). By contrast, in cells transfected with APP shRNA, exposure to 1 μM glutamate did not significantly change either the length of the AIS (Fig. 3*H*) or its distance from the cell soma (Fig. 3*G*). APP shRNA alone induced a modest, but nonsignificant, increase in the length of the AIS and had no effect on the soma to AIS distance. These data suggest that APP is required for the glutamate-dependent changes in AIS structure.

Enhanced APP expression would be expected to increase APP proteolytic processing and hence to increase levels of the Aβ peptide. This raised the possibility that the effects of APP expression were indirect and mediated through its breakdown product, Aβ. To test this idea, fibrillar Aβ [Aβ (f)] and Aβ oligomers [Aβ (o)] were prepared from commercially available peptide by standard protocols (Mehta et al., 1998; Zhu et al., 2019). The level of aggregation was verified by Western blot using the 6E10 antibody as a probe (Fig. 4*A*). Both types of Aβ preparations were then used to treat DIV14 neuronal cultures. After 24 h, the cells were fixed and immunostained for AIS scaffold proteins and synaptic protein markers. Neuronal number remained unchanged after Aβ treatment, even while the density of synapses was reduced (Fig. 4*B*). Despite the loss of synapses, however, the length of the AIS remained unaffected in both the Aβ (f) and Aβ (o) treated cultures (Fig. 4*C*,*D*). The distance of the proximal end of the AIS from the cell soma likewise showed no significant change (Fig. 4*E*).

To determine whether the mouse neurons we were using for our Aβ assays accurately reflected the situation in the human brain, we used human iPSC-derived neuronal cultures to test the effect of Aβ on the dimensions of the AIS of human neurons. Four to 5 weeks after neuronal induction (see Materials and Methods), the mature human iPSC-derived neurons were treated with Aβ (o) for 24 h followed by immunostaining for the neuronal marker, TuJ1, and the AIS marker, AnkG (Fig. 4*F*). In untreated cultures, the average length of the AIS (~30 μm) was similar to the length of the AIS in cultured mouse neurons (~35 μm). The distance from the cell soma to the most proximal portion of the AIS was slightly greater in human neurons (~15 μm) compared with mouse primary neurons (~11 μm), but remarkably similar given the differences in the two preparations. The similarities carried over into the Aβ response. Neither the length of the AIS (Fig. 4*G*) nor its distance from the soma (Fig. 4*H*) was altered in the human neurons by the application of Aβ. These data suggest that the alterations of the AIS are caused by the overexpression of APP directly and not indirectly through increased levels of Aβ.

The AD brain has evidence of increased calpain protease activity (Saito et al., 1993; Sheehan et al., 1997; Leissring et al., 2000), as do AD mouse models (Kurbatskaya et al., 2016; Ahmad et al., 2018). Both AnkG and βIV spectrin are calpain substrates, and their proteolytic cleavage leads to the dispersion of the ion channels normally clustered at the AIS (Schafer et al., 2009; Greer et al., 2013). Glutamate stimulation would be expected to activate NMDA channels, increase intracellular calcium, and thus alter calcium dynamics, although there are questions as to how this happens (Woods and Padmanabhan, 2012). To test whether the reduction of AIS length we observed was because of the activation of calpain, we treated primary cultures of WT mouse neurons with the calpain inhibitor, PD150606 (1 mM), then transfected the neurons with APP_{Swe}. After calpain inhibition, we found that the reduction in AIS length was significantly less than in cells without inhibitor (Fig. 4*I*,*J*). Immunocytochemistry with 6E10 showed that the same amount of APP was expressed, and its distribution within the cells was comparable in the presence and absence of PD150606. It should be noted, however, that the length of the AIS was only partially restored by this treatment (Fig. 4*I*). The suggestion is that, while calpain plays a role in the APP effects, there are likely other mechanisms involved.

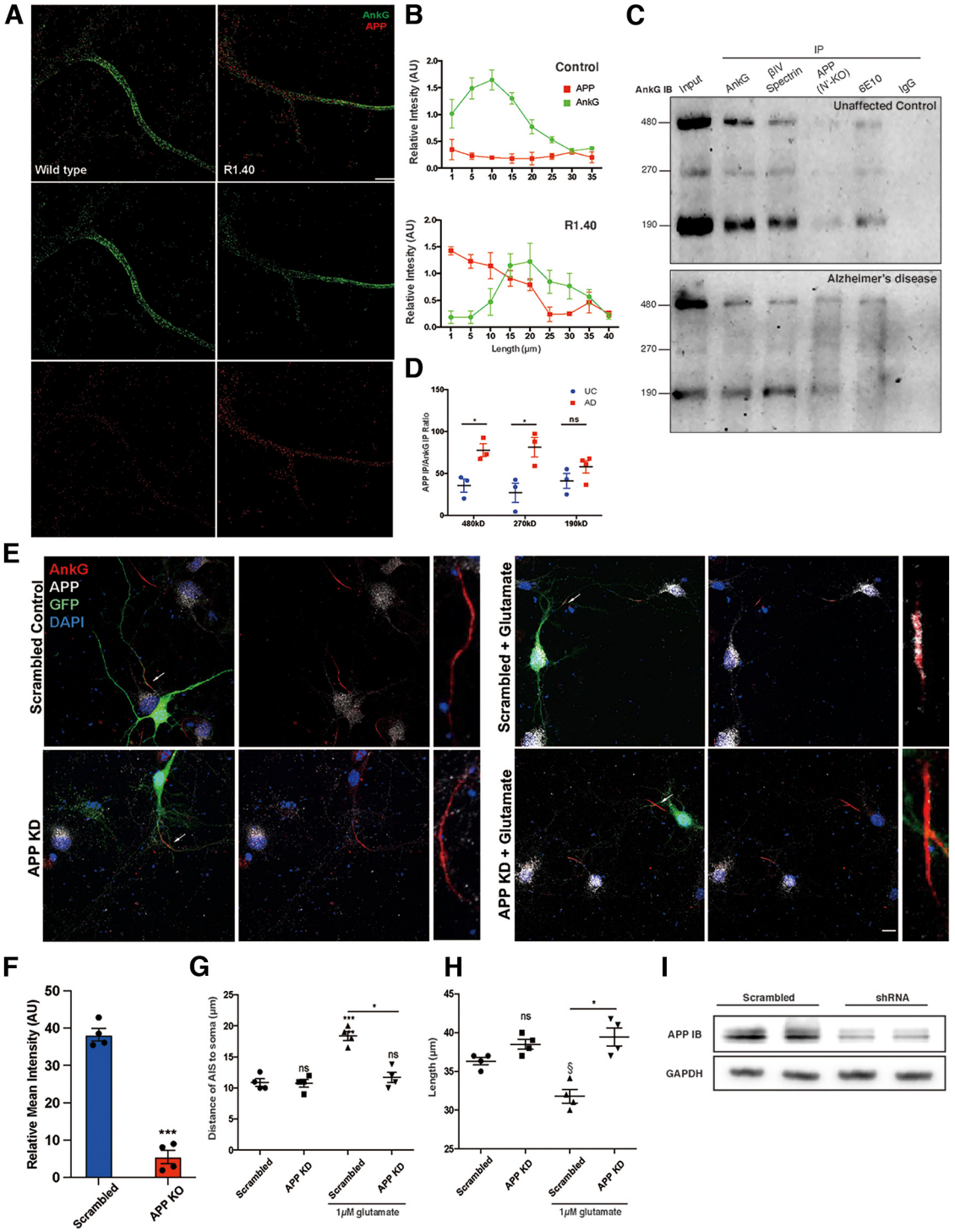

Figure 3. APP interacts with the AIS scaffold proteins and is required for glutamate-induced changes. ***A***, Super-resolution imaging of AnkG (green) and N′APP (red) in cultured neurons from WT and R1.40 mice fixed at DIV14. Scale bar, 5 μm. ***B***, Intensity (relative gray value) of APP (red) and AnkG (green) in the AIS as a function of distance from the cell body. ***C***, Representative Western blots of coimmunoprecipitations of cortical (BA9) lysates from UC and AD brains probed with AnkG antibody. Antibodies used for the precipitation are noted at the top of each lane. ***D***, Intensity of the indicated molecular weight bands after APP (N′KO) precipitation (lane 4) normalized to the intensity of the of the same molecular weight bands in the AnkG precipitation (lane 2). ***E***, Primary cortical neurons were treated with APP shRNA 48 h before treatment with 1 μM glutamate for 24 h, fixed, and immunostained for AnkG (red) and APP (N-terminus, KO-validated, gray). Insets, Enlargements of the fiber indicated by the white arrows in the panels in the most left column. Scale bar, 10 μm. ***F***, Quantification of the cellular intensity of APP immunofluorescent signal in scrambled and APP KD cells. ***G***, Distance from the cell soma to the proximal end of the AIS after the indicated treatments. ***H***, Length of the AIS after the indicated treatments. ***I***, Western blot of N′APP using the cell lysates from primary neurons with *in vitro* APP knockdown and scrambled control. Data are mean ± SEM. $*p < 0.05$; $***p < 0.0001$; unpaired *t* test. $n = 4$ batches of independent cultures. At least 20 neurons were quantified for each replicate.

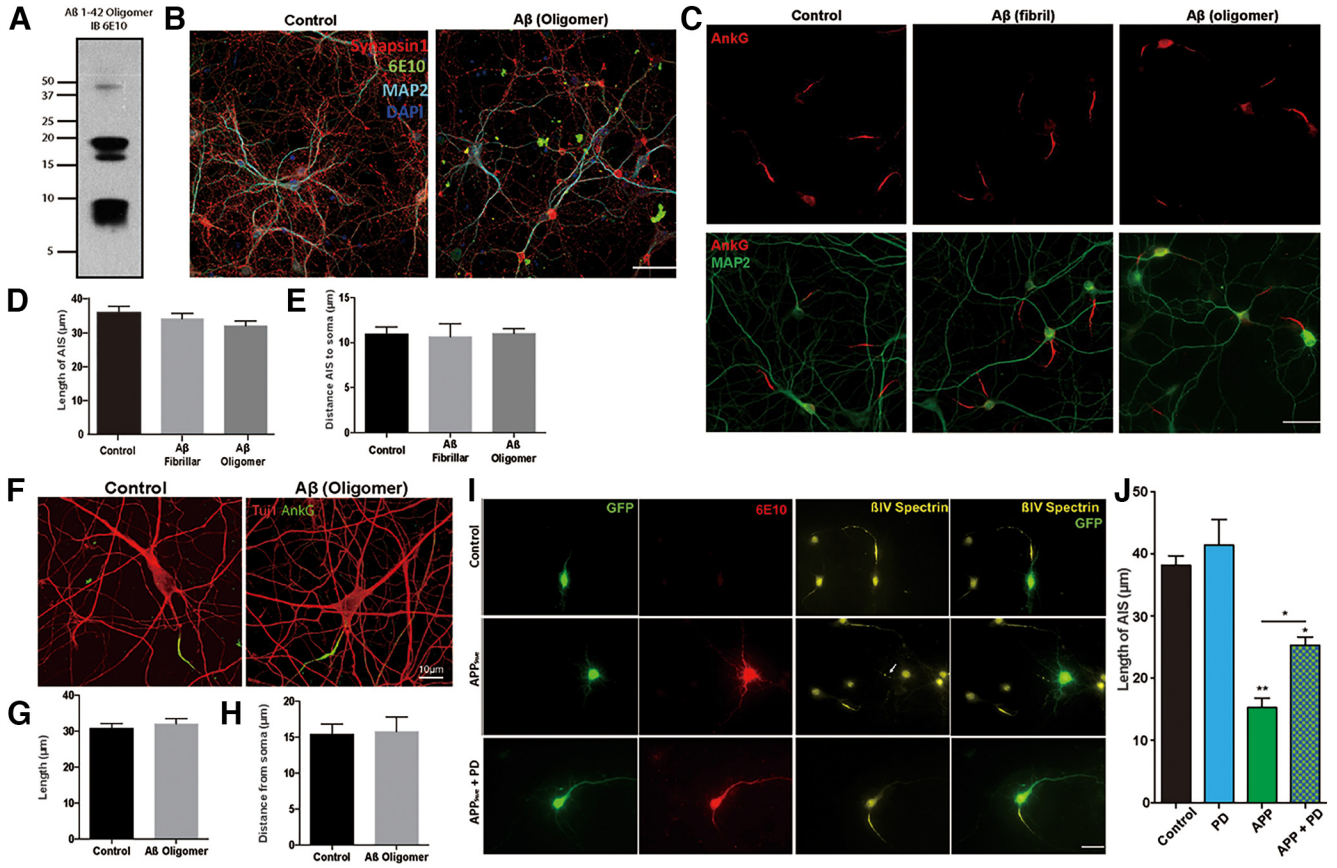

Figure 4. APP-induced changes in the AIS are independent of Aβ but partially dependent on calpain activity. ***A***, Western blot of the Aβ oligomer sample used (blotted with the 6E10 antibody). ***B***, DIV14 primary cultured neurons treated with Aβ oligomer (1 μM) for 24 h, then fixed and immunolabeled for Synapsin1 (red), Aβ (6E10 antibody, green), and MAP2 (cyan). Nuclei were labeled with DAPI (blue). Scale bar, 20 µm. ***C***, DIV14 neurons treated with fibrillar or oligomeric Aβ for 24 h, then immunolabeled for AnkG (red) to reveal the AIS and for MAP2 (green). Scale bar, 25 µm. ***D***, Quantification of the average length of the AIS in cultures, such as those in ***C***. ***E***, Quantification of the distance of the AIS from the soma. ***F***, Glutamatergic neurons were generated from human iPS cells. After 4 weeks maturation, the cells were treated with Aβ oligomers for 24 h before fixation and immunostaining with Tuj1 (red) and AnkG (green). Scale bar, 10 µm. ***G***, Quantification of the AIS length in cultures, such as that shown in ***F***. ***H***, Quantification of the distance of the AIS from the soma. ***I***, DIV7 neurons transfected with APP_{Swe} plasmid with or without the calpain inhibitor, PD150606 (PD), for 2 d and immunolabeled with the AIS marker βIV spectrin (yellow) and APP (6E10, red). GFP labels the transfected cells and is shown in green. Scale bar, 20 µm. ***J***, Quantification of the length of the AIS from the experiment shown in ***I***. Symbols over individual bars represent significance of difference from control. Data are mean ± SEM. *$p < 0.05$; **$p < 0.001$; one-way ANOVA. $n = 4$ batches of independent cultures.

The APP-induced changes in AIS structure are reflected in neuronal activity

Previous studies suggest that, by decreasing AIS length and increasing its distance from the cell body, the elevated levels of APP should raise the threshold for action potential generation (Grubb and Burrone, 2010a; Kuba et al., 2014). This is predicted to decrease the activity of the neuronal networks that establish themselves among cultured dissociated neurons. To test this prediction, we infected neuronal cultures on DIV10 with a lentivirus expressing GCaMP8f, a calcium sensor that is widely used to monitor activity in living nerve cells (Zhang et al., 2021). Sister cultures were coinfected with GCaMP8f plus an APP expressing virus. At DIV14, APP-infected cells (e. g., the cell in the white box and the arrow in Fig. 5*B*) showed noticeably higher mCherry signal than that in the nearby non–APP-transfected cells in the same culture. This was true in both the cell body and the processes. The chemograph showed the change of the GCaMP8f signal changes in the green and red boxes from Figure 5*B*. We then monitored either the total GCaMP8f signal (ΔF/F) over a 15 s time frame (Fig. 5*C–E*) or the total number of GCaMP8f flashes over the same time period (Fig. 5*D*,*E*). Both measurements were reduced showing that, as predicted, APP overexpression reduces the activity of neuronal cultures.

The AIS in AD: *in vivo* data

The data described thus far have come from *in vitro* assays. To ask whether similar results would be found *in vivo*, we compared the AIS in cryostat sections from the brains of WT and R1.40 mice. R1.40 mice carry a human APP_{Swe} transgene in addition to the endogenous (WT) mouse *App* gene. *In vivo*, the measured length of the WT AIS was shorter (10-15 µm) than it was *in vitro* (30-35 µm). Even with this difference, the relative decrease in the length of the AIS of R1.40 neurons was readily apparent (Fig. 6*A*). The reduction was seen in all regions of cortex but failed to reach statistical significance in more posterior samples (Fig. 6*B*). To rule out the possibility that a change in orientation was the cause of this difference, we also took AIS measurements of cortical neurons in the coronal plane and obtained similar results (Fig. 6*C*). As an additional control, we compared the apparent length of the AIS measured in cryostat sections of different thicknesses. While we observed a modest 20%-25% increase in the measured AIS length in 20 µm sections compared with the 10 µm used above, there was no change in the relative difference (or its statistical significance) between the AIS of WT and R1.40 neurons (data not shown). The changes in AIS length in the R1.40 mouse were found, although the density of the AIS did not differ between the two genotypes (Fig. 6*D*,*E*). We also quantified the AIS lengths

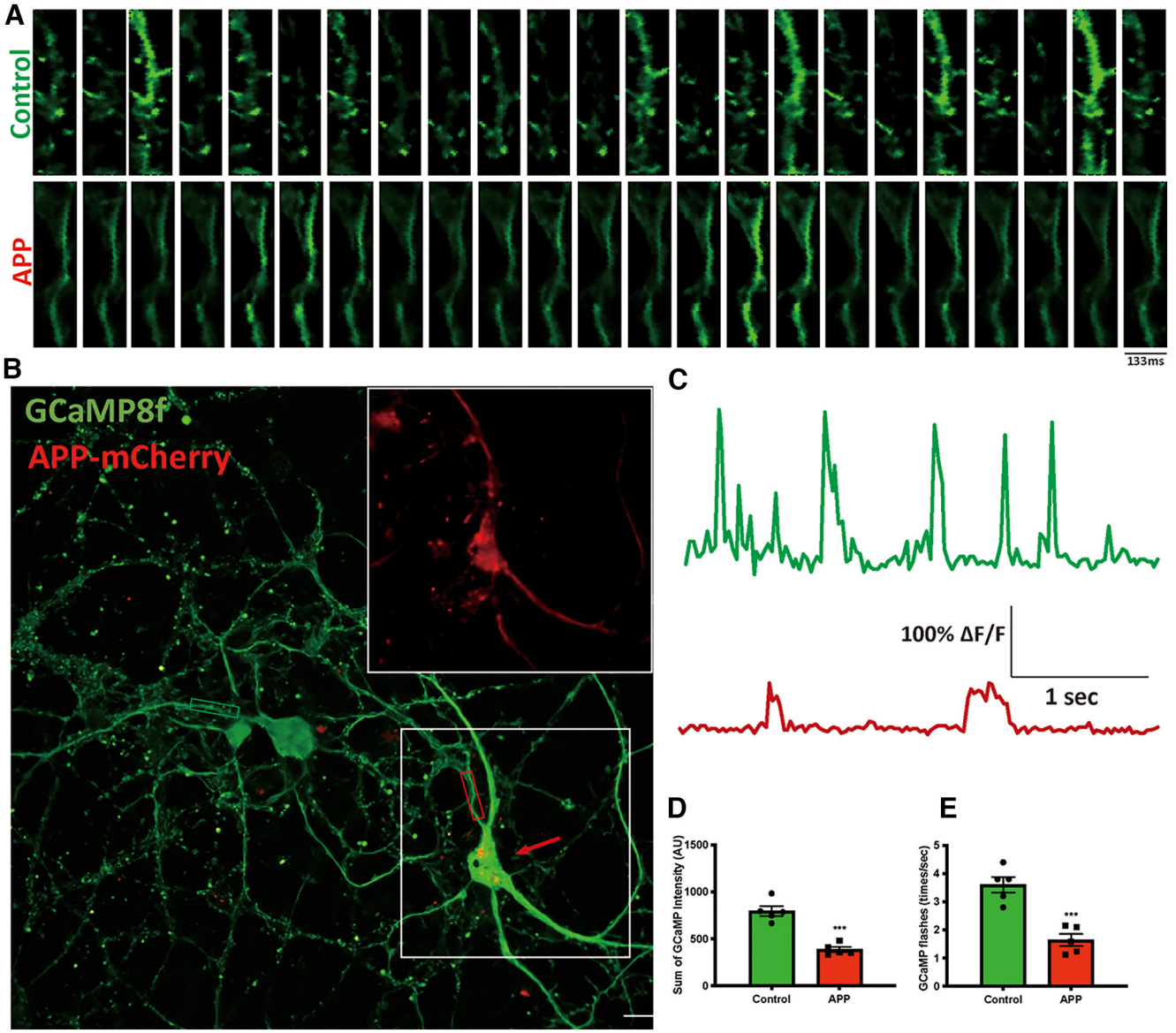

Figure 5. Impact of APP on neuronal network activity. ***A***, Time-series chemograph of representative neurites from GCaMP8f lentivirus-infected neurons. In each row, the frames are images of the same fibers taken 133 ms apart. Top row (Con) represents the fiber of a cell infected with GCaMP8f alone. Note the low background GCaMP8f signal relative to the signal from the fiber during an event. Bottom row represents the fiber of a cell infected with GCaMP8f and APP-mCherry identified by the white box in ***B***. Brightness and contrast of each row of images were equally adjusted based on optimal visualization to illustrate the GCaMP fluorescent signal. ***B***, Images of the two cells whose fibers are shown in ***A***. The cell identified in the white box has been infected with both GCaMP8f (green) and APP-mCherry (red, inset). The other cell has been infected with GCaMP8f, but not APP (no red signal; not shown). The imaged fibers are indicated with small boxes: red represents the APP-mCherry neurite; green represents the GCaMP8f-only neurite. ***C***, Representative traces of the ΔF/F ratio of the control fiber (green) and the APP-infected fiber (red). Both the relative increase in fluorescent signal during a flash and the time between flashes are affected by APP expression. ***D***, Sum of the GCaMP8f signal during the entire 15 s recording period. ***E***, The total number of flashes during the entire 15 s recording period. Each point represents a different fiber from a different cell.

of R1.40 pyramidal cells of the CA fields of the hippocampus (Fig. 6*F*,*H*) and found them to be significantly shorter than WT in both the sagittal (Fig. 6*F*) and coronal planes (not shown). Unlike the neocortex, however, the density of AIS was reduced in the CA fields of R1.40 mice (Fig. 6*G*).

The *in vitro* data demonstrated that exposure to Aβ peptides alone does not affect the properties of the AIS. Qualitative observations of β4 spectrin/APP (Clone: 6E10) double-immunolabeled material supported this view as they revealed no obvious bending of the AIS in or near cortical amyloid plaques (Fig. 7*A*). R1.40 mice start to build up plaques in the frontal cortex by 13.5 months. By 18 months, plaque density has increased significantly (Lamb et al., 1997; Kulnane and Lamb, 2001; Lehman et al., 2003). We thus measured the density and length of the AIS in 18 month R1.40 mouse frontal cortex. We computed both values in areas defined by three concentric rings centered on 6E10-positive Aβ plaques (Fig. 7*B*), a method established by Marin et al. (2016). We found no statistically significant association between AIS length (Fig. 7*C*) or density (Fig. 7*D*) and the distance of the AIS from the center of a plaque. Thus, consistent with our *in vitro* findings, the reduction of AIS length was not sensitive to the presence of amyloid.

To test whether the situation in human AD was similar to the R1.40 mouse AD model, we turned to human postmortem brain samples. We chose Brodmann Area 9 (BA9) as our test region. We immunostained 10 µm cryostat sections for MAP2, APP (N-terminus), and AnkG. In material from UCs (Fig. 7*A*), the AIS was well stained, and many (though not all) could be clearly

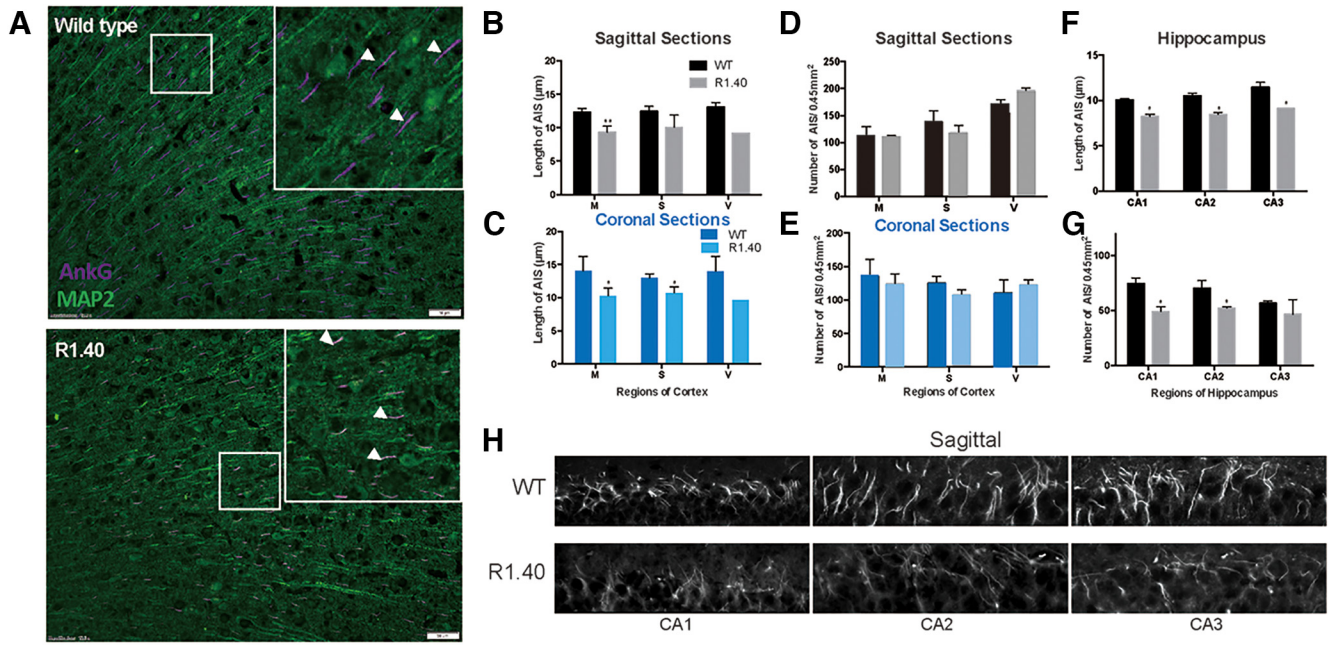

Figure 6. Alterations in the AIS in R1.40 cortex and hippocampus. ***A***, Cryostat sections from 18-month-old WT and R1.40 frontal cortex immunostained with MAP2 (green) and AnkG (purple) antibodies. Scale bar, 50 μm. ***B***, Length of AIS measured in sagittal sections from motor (M), somatosensory (S), and visual (V) cortex in 18-month WT and R1.40 mice. ***C***, Length of AIS measured in coronal sections from 18-month WT and R1.40 mice. ***D***, AIS density (number of AIS/0.45 mm^2 field) in motor (M), somatosensory (S), and visual (V) cortex measured in sagittal sections. ***E***, AIS density in motor (M), somatosensory (S), and visual (V) cortex measured in coronal sections. ***F***, Length of the AIS of pyramidal neurons of the hippocampus of WT and R1.40 mice measured in sagittal section. ***G***, Density of the AIS of CA1, CA2, and CA3 pyramidal neurons of the hippocampus of WT and R1.40 mice measured in sagittal sections. ***H***, Immunolabeling of the AIS of hippocampal CA1, CA2, and CA3 pyramidal cells in WT and R1.40 mice. Scale bar, 10 μm. Data are mean ± SEM. $*p < 0.05$; $**p < 0.001$; unpaired *t* test. $n = 4$ (2 females and 2 males for each genotype).

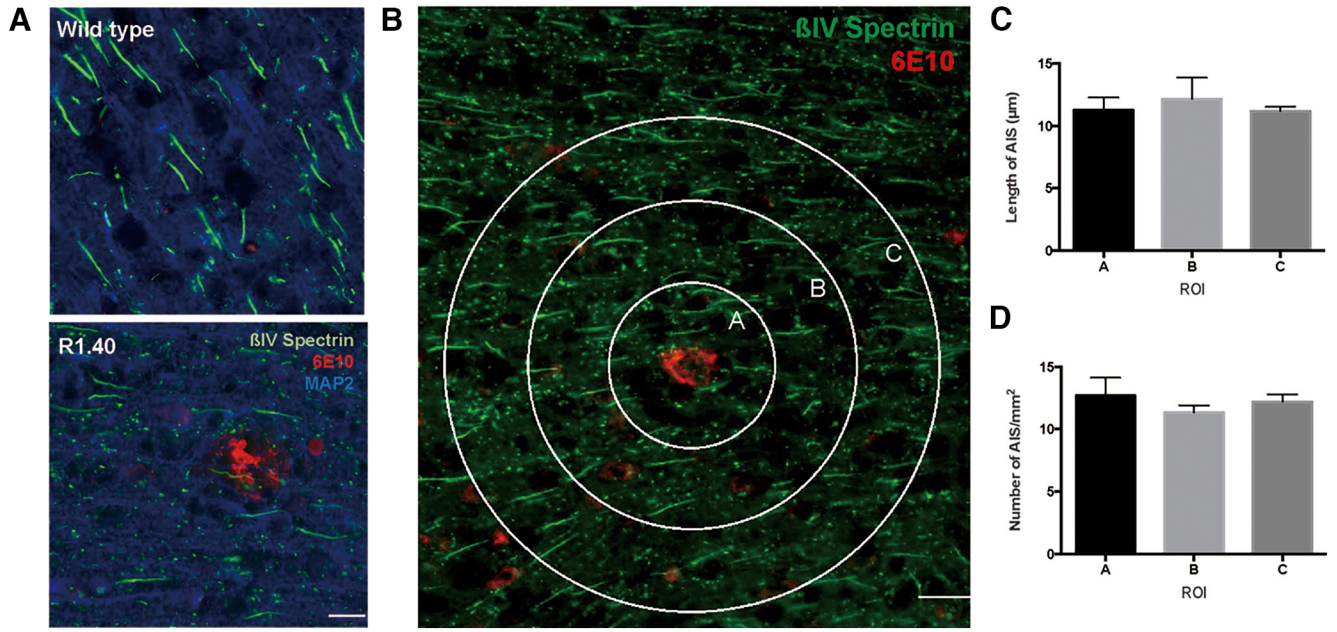

Figure 7. Properties of the AIS are unchanged in the vicinity of a plaque. ***A***, Cortex of 18-month WT and R1.40 mouse immunolabeled for βIV-spectrin (green), APP (6E10 antibody, red), and MAP2 (blue). Scale bar, 10 μm. ***B***, Three concentric rings (50, 100, and 150 μm in diameter) were centered on an Aβ ($6E10^+$) plaque and used to define three ROIs (A–C). AISs were immunostained using antibodies against βIV spectrin (green). Scale bar, 20 μm. ***C***, Quantification of the length of the AIS in the three regions. ***D***, Quantification of the density of AIS in the three regions. The differences shown in ***C*** and ***D*** were not significant by one-way ANOVA. $n = 3$. Data are mean ± SEM.

associated with their neuron of origin (Fig. 8*Ai*). While in control specimens the levels of intracellular APP immunoreactivity were low, a few neurons displayed elevated staining (Fig. 8*A*, yellow arrow). In cells with low levels of APP, an associated AIS could often be identified (Fig. 8*Aii*). For neurons with elevated APP, however, we could rarely identify its associated AIS. To be sure, the thickness of the cryostat sections was less than the average diameter of a neuron. Thus, for any given neuron, the AIS

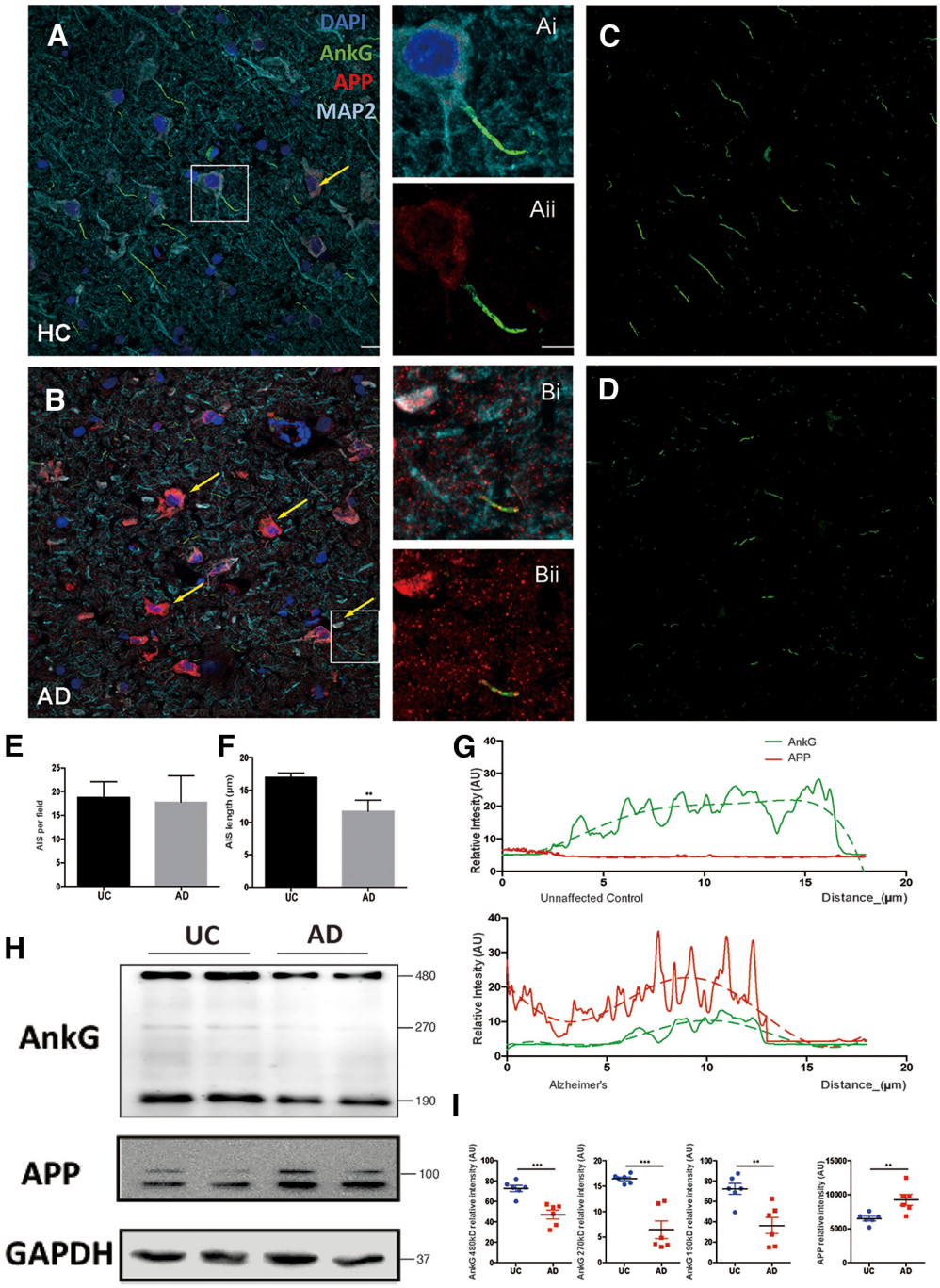

Figure 8. The impact of sporadic AD on the properties of the AIS. ***A***, Immunolabeling of the AIS in neurons from BA9 of a healthy control (HC) using antibodies against AnkG (green), the APP N-terminus (N′APP, red), MAP2 (cyan), and DAPI (blue). Yellow arrows indicate examples of neurons with increased intracellular APP. ***Ai***, Enlargement of the area shown in the white box. ***Aii***, Same area as in ***Ai***, but showing only the APP and AnkG labels. ***B***, Immunolabeling of the AIS in neurons from BA9 of a case of sporadic AD. Yellow arrows indicate examples of neurons with increased intracellular APP. ***Bi***, Enlargement of the area shown in the white box. ***Bii***, Same area as in ***Bi***, but showing only the APP and AnkG labels. ***C***, Same field as in ***A***, but showing only the AnkG channel. ***D***, Same field as in ***B***, but showing only the AnkG only channel. Scale bars, 10 μm. ***E***, The density of AIS in the BA9 region of UCs and sporadic AD. ***F***, The length of the AIS in the BA9 region of UCs and sporadic AD. ***G***, Intensity of AnkG immunolabeling along the AIS shown in ***Aii*** and ***Bii*** (AnkG, green lines and APP, red lines). Green and red dashed lines indicate the polynomial regression curve of the intensity of AnkG and APP, respectively. ***H***, Western blots of BA9 lysates of age-matched UC and AD brains probed with AnkG and APP antibodies. ***I***, Quantification of the band intensity of the Western blot data shown in ***H***. Data are mean ± SEM. $^{**}p < 0.001$; $^{***}p < 0.0001$; unpaired *t* test. $n = 6$.

could well have been located in an adjacent section. The consistency of the finding, however, was striking and it was amplified by the situation in the AD material.

In all 6 AD cases examined, the presence of amyloid plaques was readily observed. Though less often discussed in the literature, we found an equally impressive increase in the level of background staining. This background can be clearly seen in Figure 8*Bi*, 8*Bii* (insets). As each of the AD cases was sporadic in nature, the elevated levels of APP immunostaining were most probably a function of age and environmental factors. In addition to the higher APP background, virtually every neuron in cortex presented with strong intracellular APP immunoreactivity (Fig. 8*B*, yellow arrows). Plus, as would be predicted from the few high APP-expressing neurons in the UCs, we could almost

never define a cell of origin for any of the AIS present in an AD brain section.

The AnkG channel from the merged images (Fig. 8*A*,*B*) was used to quantify the dimensions of the AIS in UCs (Fig. 8*C*) and in AD cases (Fig. 8*D*). It was notable that, although the size of human brain is much larger than that of the mouse brain, the length of the AIS of human prefrontal neurons (10-18 μm) was only slightly longer than that found in the mouse (10-15 μm). By contrast, the average density of AIS in the human material was about one-fifth of that found in mouse (Fig. 8*E*). Further, just as we found in the R1.40 transgenic mouse, the average length of the AIS was decreased by about one-third in the AD brain compared with UCs (Fig. 7*F*). Double-staining with AnkG and N-term APP plainly showed that, in all AD cases, the APP protein had infiltrated the AIS region (Fig. 8*Bii*). An important distinction with the mouse, however, was that there was little evidence of a reciprocal gradient of APP and AnkG. In the R1.40 mouse, the excess APP appeared to shift the peak of AnkG nearly 10 μm distally from that seen in WT. In the human, although the intensity and total length of AnkG staining region were reduced, the shift was less apparent (Fig. 8*G*, compare with green symbols in Fig. 3*C*).

To obtain a more global picture of these changes, we performed Western blots of APP and Ankyrin G using lysates prepared from cryostat sections of the same blocks of human BA9 tissue used for immunocytochemistry (Fig. 8*H*). Not unexpectedly, we found that the levels of APP protein were considerably higher on average in the AD brain than in UCs (Fig. 8*I*). The increase was statistically significant and quantitatively similar to the increase seen in APP levels in the R1.40 mouse brain. By contrast, the overall levels of Ankyrin G protein were significantly decreased in AD brain compared with UCs, significantly so for both the 480 and 270 kDa bands (Fig. 8*I*).

Discussion

Our findings reveal several new and unexpected roles of the full-length APP protein in brain function. First, we found that a sustained increase in neuronal activity leads to a rapid increase in *App* gene expression. Second, we demonstrated that elevated levels of APP protein, whether caused by glutamate, APP overexpression, or an APP transgene, led to two important changes in the AIS: it shortens in length and shifts in position away from the cell body. Third, we showed that these changes in AIS position and length are associated with the predicted decrease in neuronal network activity. Fourth, we showed that the effect on AIS length is observed in neurons both *in vivo* and *in vitro*. Finally, we confirmed that in humans with sporadic AD cortical neurons have elevated levels of APP protein, and that portions of this excess APP invade the AIS domain. This increased APP is associated with a significant shortening of the AIS compared with UCs.

The AIS is an important yet highly dynamic region of a neuron. Alterations of the length and position of the AIS are activity-dependent and, in turn, affect neuronal activity (Grubb and Burrone, 2010b; Huang and Rasband, 2018; Leterrier, 2018). As the site of action potential initiation, even subtle changes in the AIS can have measurable effects on neuronal excitability (Grubb and Burrone, 2010a; Kuba et al., 2010; Kuba, 2012; Atapour and Rosa, 2017; Kneynsberg and Kanaan, 2017). A longer AIS, or one more proximal to the cell body, will result in a more excitable neuron because of a lower action potential firing threshold. The reverse situation is also true. When the length of the AIS decreases or it shifts to a more distal position along the axon, neuronal activity is decreased (Grubb and Burrone, 2010a; Rasband, 2010). While this correlation between AIS structure and electrophysiological function has been clear, the mechanisms that link changes in AIS structure with activity have remained largely unknown. Correlations with altered calcium levels (Evans et al., 2013) and the resulting activation of calpain, a protease capable of cleaving both Ankyrin G and βIV spectrin, offer one possible explanation (Schafer et al., 2009). Yet the studies described here using calpain inhibition suggest that calpain itself can provide only a partial explanation of the observed phenomena.

The actions of APP we have documented offer a compelling, additional mechanism to explain the correlation between neuronal activity and AIS behavior. With immunocytochemistry in both mouse and human, we showed that, in a mature AIS, APP is in close apposition to both ankyrin G and βIV spectrin. The results of the coimmunoprecipitation experiments confirm this by showing that APP physically interacts with both major scaffolding proteins. The association is found with human as well as with mouse APP proteins. Manipulating the levels of APP either genetically or through glutamate stimulation shows that this physical interaction is coupled with structural consequences for the AIS. With increased neuronal activity, *App* gene transcription is rapidly upregulated, and protein levels follow rather closely. The transcriptional response is mostly likely the key to this regulation as the APP protein has a relatively short half-life (Xiao et al., 2015). Coupled with the electrophysiological consequences of changes in AIS structure, the dynamic nature of the transcriptional response suggests that, under normal conditions, APP acts as a modulator on neuronal excitability. When neuronal activity increases, APP levels rise causing the distance between the AIS and the soma to increase and the length of the AIS to decrease. The overall effect is to reduce the neuron's firing threshold and thus serve as a protective mechanism.

The data from human AD neurons and mouse AD models suggest that, beyond its contribution to normal neuronal activity, the AIS may also play a role in neurodegenerative disease. Elevated APP levels, such as those found in AD, drive the same changes in AIS position and length, as does increased neuronal activity. The relevance of this finding to AD is enhanced by data showing that $hAPP_{Swe}$ has effects on the AIS that are more dramatic than those of WT hAPP. The effects are cell autonomous and mediated by endogenous full-length APP protein, not by exogenous Aβ. Addition of Aβ to the culture medium (oligomers or fibrils) has no effect on the AIS of either human or mouse neurons. Plus, the length of the AIS in the neurons of the mouse brain is unaffected by its proximity to an amyloid deposit. The immunoprecipitation data further support the connection between the dynamics of the AIS and the symptoms of AD. Antibody to APP pulls down ankyrin G and βIV spectrin from both human and mouse brain lysates (Fig. 3*C*). The human observation is particularly informative as the AD cases were all sporadic; the increased levels of APP would be exclusively WT in structure. The retarded development of the AIS in R1.40 cultures may have additional implications for the full clinical picture of AD. AD has long been recognized as having a developmental component, with intellectual performance in youth inversely related to the risk of dementia in old age (Snowdon et al., 1996; Whalley et al., 2000). In this light, the slow development and shorter length of the AIS in cultured R1.40 neurons suggest that elevated APP expression may be one explanation for this connection.

In sporadic AD, we speculate that the aging process leads to a relentless increase in the damage experienced by neurons. As APP is a damage response protein, this results in a chronic elevation in the levels of APP. We speculate that this lifetime accumulation of APP, worsened by hyperexcitability, irritation because of inflammation, vascular problems, or a traumatic injury, eventually tips the system into a disease state. The levels of APP never return to normal leading to a sustained shift in the position of the AIS away from the cell body and a reduction in its length. Both changes would have the effect of lowering neuronal excitability. We found that the reduction of AIS length compared with control animals was uniformly distributed throughout the R1.40 frontal cortex, which emphasizes that the changes are APP-dependent, not Aβ-dependent. The effects on the AIS can be assumed to occur throughout the nervous system, not only in proximity to amyloid plaques. Our model further predicts that familial AD mutations in APP exacerbate the normal age-associated vulnerabilities, leading to an earlier age of onset, as is clinically observed.

One important observation that does not fit our proposed model is that hyperexcitability and epileptic activity are features of both AD and its mouse models (Di Lazzaro et al., 2004a, 2004b; Palop et al., 2007; Minkeviciene et al., 2009; Pennisi et al., 2011), yet one of the phenotypes of APP-overexpressing neurons is a reduced probability of firing. Although only speculation, we would propose that the APP overexpression and its effects on the AIS are not experienced equally by all brain regions and that those regions, or neurons, that are spared attempt to compensate for reduced network activity increasing their firing frequency. This is consistent with the heterogeneity we observed in our human material in both the APP intensity in different neurons and the infiltration of APP in different individual AIS.

We note that, while mutations of APP leading to familial AD are consistent with an Aβ-dependent disease mechanism, the Alzheimer's genetic data formally identify only APP; the involvement of Aβ is inferential. The *PSEN1* and *PSEN2* familial AD genes fortify the Aβ argument, but only indirectly as the γ-secretase has dozens of substrates apart from APP. We propose that consideration be given to the idea that the actions of the full-length APP protein on the AIS and the resultant disruption of network activity provide an alternative explanation for the APP genetic data. This would revise our disease models and offer novel therapeutic approaches to halt the advance of AD.

References

Ahmad F, Das D, Kommaddi RP, Diwakar L, Gowaikar R, Rupanagudi KV, Bennett DA, Ravindranath V (2018) Isoform-specific hyperactivation of calpain-2 occurs presymptomatically at the synapse in Alzheimer's disease mice and correlates with memory deficits in human subjects. Sci Rep 8:13119.

Atapour N, Rosa MG (2017) Age-related plasticity of the axon initial segment of cortical pyramidal cells in marmoset monkeys. Neurobiol Aging 57:95–103.

Cao X, Sudhof TC (2001) A transcriptionally [correction of transcriptively] active complex of APP with Fe65 and histone acetyltransferase Tip60. Science 293:115–120.

Colbert CM, Johnston D (1996) Axonal action-potential initiation and Na^+ channel densities in the soma and axon initial segment of subicular pyramidal neurons. J Neurosci 16:6676–6686.

Costa BM, et al. (2009) N-methyl-D-aspartate (NMDA) receptor NR2 subunit selectivity of a series of novel piperazine-2, 3-dicarboxylate derivatives: preferential blockade of extrasynaptic NMDA receptors in the rat hippocampal CA3-CA1 synapse. J Pharmacol Exp Ther 331:618–626.

Di Lazzaro V, et al. (2004a) Motor cortex hyperexcitability to transcranial magnetic stimulation in Alzheimer's disease. J Neurol Neurosurg Psychiatry 75:555–559.

Di Lazzaro V, et al. (2004b) The physiological basis of transcranial motor cortex stimulation in conscious humans. Clin Neurophysiol 115:255–266.

Evans MD, Sammons RP, Lebron S, Dumitrescu AS, Watkins TB, Uebele VN, Renger JJ, Grubb MS (2013) Calcineurin signaling mediates activity-dependent relocation of the axon initial segment. J Neurosci 33:6950–6963.

Fisher S, Gearhart JD, Oster-Granite ML (1991) Expression of the amyloid precursor protein gene in mouse oocytes and embryos. Proc Natl Acad Sci USA 88:1779–1782.

Frederikse PH, Garland D, Zigler JJ, Piatigorsky J (1996) Oxidative stress increases production of beta-amyloid precursor protein and beta-amyloid (Abeta) in mammalian lenses, and Abeta has toxic effects on lens epithelial cells. J Biol Chem 271:10169–10174.

Furukawa K, Sopher BL, Rydel RE, Begley JG, Pham DG, Martin GM, Fox M, Mattson MP (1996) Increased activity-regulating and neuroprotective efficacy of α-secretase-derived secreted amyloid precursor protein conferred by a C-terminal heparin-binding domain. J Neurochem 67:1882–1896.

Gao Y, Pimplikar SW (2001) The gamma-secretase-cleaved C-terminal fragment of amyloid precursor protein mediates signaling to the nucleus. Proc Natl Acad Sci USA 98:14979–14984.

Gentleman SM, Nash MJ, Sweeting CJ, Graham DI, Roberts GW (1993) β-Amyloid precursor protein (βAPP) as a marker for axonal injury after head injury. Neurosci Lett 160:139–144.

Goldgaber D, Lerman MI, McBride OW, Saffiotti U, Gajdusek DC (1987) Characterization and chromosomal localization of a cDNA encoding brain amyloid of Alzheimer's disease. Science 235:877–880.

Greenamyre JT, Young AB (1989) Excitatory amino acids and Alzheimer's disease. Neurobiol Aging 10:593–602.

Greer JE, Hånell A, McGinn MJ, Povlishock JT (2013) Mild traumatic brain injury in the mouse induces axotomy primarily within the axon initial segment. Acta Neuropathol 126:59–74.

Grubb MS, Burrone J (2010a) Activity-dependent relocation of the axon initial segment fine-tunes neuronal excitability. Nature 465:1070–1074.

Grubb MS, Burrone J (2010b) Building and maintaining the axon initial segment. Curr Opin Neurobiol 20:481–488.

Hedstrom KL, Ogawa Y, Rasband MN (2008) AnkyrinG is required for maintenance of the axon initial segment and neuronal polarity. J Cell Biol 183:635–640.

Huang CY, Rasband MN (2018) Axon initial segments: structure, function, and disease. Ann NY Acad Sci 1420:46–61.

Jenkins SM, Bennett V (2001) Ankyrin-G coordinates assembly of the spectrin-based membrane skeleton, voltage-gated sodium channels, and L1 CAMs at Purkinje neuron initial segments. J Cell Biol 155:739–746.

Johnson JW, Kotermanski SE (2006) Mechanism of action of memantine. Curr Opin Pharmacol 6:61–67.

Kang J, et al. (1987) The precursor of Alzheimer's disease amyloid A4 protein resembles a cell-surface receptor. Nature 325:733–736.

Kibbey MC, Jucker M, Weeks BS, Neve RL, Van Nostrand WE, Kleinman HK (1993) beta-Amyloid precursor protein binds to the neurite-promoting IKVAV site of laminin. Proc Natl Acad Sci USA 90:10150–10153.

Klevanski M, et al. (2015) The APP intracellular domain is required for normal synaptic morphology, synaptic plasticity, and hippocampus-dependent behavior. J Neurosci 35:16018–16033.

Kneynsberg A, Kanaan NM (2017) Aging does not affect axon initial segment structure and somatic localization of tau protein in hippocampal neurons of Fischer 344 rats. eNeuro 4:ENEURO.0043-17.2017.

Kole MH, Ilschner SU, Kampa BM, Williams SR, Ruben PC, Stuart GJ (2008) Action potential generation requires a high sodium channel density in the axon initial segment. Nat Neurosci 11:178–186.

Kuba H (2012) Structural tuning and plasticity of the axon initial segment in auditory neurons. J Physiol 590:5571–5579.

Kuba H, Oichi Y, Ohmori H (2010) Presynaptic activity regulates Na^+ channel distribution at the axon initial segment. Nature 465:1075–1078.

Kuba H, Adachi R, Ohmori H (2014) Activity-dependent and activity-independent development of the axon initial segment. J Neurosci 34:3443–3453.

Kulnane LS, Lamb BT (2001) Neuropathological characterization of mutant amyloid precursor protein yeast artificial chromosome transgenic mice. Neurobiol Dis 8:982–992.

Kurbatskaya K, et al. (2016) Upregulation of calpain activity precedes tau phosphorylation and loss of synaptic proteins in Alzheimer's disease brain. Acta Neuropathol Commun 4:1–15.

Lamb BT, et al. (1993) Introduction and expression of the 400 kilobase amyloid precursor protein gene in transgenic mice [corrected]. Nat Genet 5:22–30.

Lamb BT, et al. (1997) Altered metabolism of familial Alzheimer's disease-linked amyloid precursor protein variants in yeast artificial chromosome transgenic mice. Hum Mol Genet 6:1535–1541.
Lee KJ, Moussa CE, Lee Y, Sung Y, Howell BW, Turner RS, Pak DT, Hoe HS (2010) Beta amyloid-independent role of amyloid precursor protein in generation and maintenance of dendritic spines. Neuroscience 169:344–356.
Lehman EJ, Kulnane LS, Lamb BT (2003) Alterations in β-amyloid production and deposition in brain regions of two transgenic models. Neurobiol Aging 24:645–653.
Leissring MA, Akbari Y, Fanger CM, Cahalan MD, Mattson MP, LaFerla FM (2000) Capacitative calcium entry deficits and elevated luminal calcium content in mutant presenilin-1 knockin mice. J Cell Biol 149:793–798.
Leterrier C (2018) The axon initial segment: an updated viewpoint. J Neurosci 38:2135–2145.
Leterrier C, Potier J, Caillol G, Debarnot C, Rueda Boroni F, Dargent B (2015) Nanoscale architecture of the axon initial segment reveals an organized and robust scaffold. Cell Rep 13:2781–2793.
Ma H, Xu J, Jin J, Huang Y, Liu Y (2017) A simple marker-assisted 3D nanometer drift correction method for superresolution microscopy. Biophys J 112:2196–2208.
Marin MA, Ziburkus J, Jankowsky J, Rasband MN (2016) Amyloid-β plaques disrupt axon initial segments. Exp Neurol 281:93–98.
Masliah E, Westland C, Rockenstein E, Abraham C, Mallory M, Veinberg I, Sheldon E, Mucke L (1997) Amyloid precursor proteins protect neurons of transgenic mice against acute and chronic excitotoxic injuries in vivo. Neuroscience 78:135–146.
Mattson MP, Cheng B, Culwell AR, Esch FS, Lieberburg I, Rydel RE (1993) Evidence for excitoprotective and intraneuronal calcium-regulating roles for secreted forms of the β-amyloid precursor protein. Neuron 10:243–254.
Mehta ND, et al. (1998) Increased Aβ42 (43) from cell lines expressing presenilin 1 mutations. Ann Neurol 43:256–258.
Minkeviciene R, et al. (2009) Amyloid β-induced neuronal hyperexcitability triggers progressive epilepsy. J Neurosci 29:3453–3462.
Miyai K, Kawauchi S, Kato T, Yamamoto T, Mukai Y, Yamamoto T, Sato S (2021) Axonal damage and behavioral deficits in rats with repetitive exposure of the brain to laser-induced shock waves: effects of inter-exposure time. Neurosci Lett 749:135722.
Mockett BG, Richter M, Abraham WC, Müller UC (2017) Therapeutic potential of secreted amyloid precursor protein APPsα. Front Mol Neurosci 10:30.
Monnet FP, Mahé V, Robel P, Baulieu EE (1995) Neurosteroids, via sigma receptors, modulate the [3H] norepinephrine release evoked by N-methyl-D-aspartate in the rat hippocampus. Proc Natl Acad Sci USA 92:3774–3778.
Muir J, Kittler JT (2014) Plasticity of GABAA receptor diffusion dynamics at the axon initial segment. Front Cell Neurosci 8:151.
Muller UC, Deller T, Korte M (2017) Not just amyloid: physiological functions of the amyloid precursor protein family. Nat Rev Neurosci 18:281–298.
Muñoz U, Sebal C, Escudero E, Esiri M, Tzartos J, Sloan C, Sadaba MC (2021) Main role of antibodies in demyelination and axonal damage in multiple sclerosis. Cell Mol Neurobiol 42:1809–1827.
Nelson AD, Jenkins PM (2017) Axonal membranes and their domains: assembly and function of the axon initial segment and node of Ranvier. Front Cell Neurosci 11:136.
Nelson AD, et al. (2020) Ankyrin-G regulates forebrain connectivity and network synchronization via interaction with GABARAP. Mol Psychiatry 25:2800–2817.
Ness S, Rafii M, Aisen P, Krams M, Silverman W, Manji H (2012) Down's syndrome and Alzheimer's disease: towards secondary prevention. Nat Rev Drug Discov 11:655–656.
Ogawa Y, Rasband MN (2008) The functional organization and assembly of the axon initial segment. Curr Opin Neurobiol 18:307–313.
Palop JJ, et al. (2007) Aberrant excitatory neuronal activity and compensatory remodeling of inhibitory hippocampal circuits in mouse models of Alzheimer's disease. Neuron 55:697–711.
Pennisi G, Ferri R, Lanza G, Cantone M, Pennisi M, Puglisi V, Malaguarnera G, Bella R (2011) Transcranial magnetic stimulation in Alzheimer's disease: a neurophysiological marker of cortical hyperexcitability. J Neural Transm (Vienna) 118:587–598.
Popova D, et al. (2023) Alcohol reverses the effects of KCNJ6 (GIRK2) non-coding variants on excitability of human glutamatergic neurons. Mol Psychiatry 28:746–758.
Priller C, Bauer T, Mitteregger G, Krebs B, Kretzschmar HA, Herms J (2006) Synapse formation and function is modulated by the amyloid precursor protein. J Neurosci 26:7212–7221.
Rama N, Goldschneider D, Corset V, Lambert J, Pays L, Mehlen P (2012) Amyloid precursor protein regulates netrin-1-mediated commissural axon outgrowth. J Biol Chem 287:30014–30023.
Rasband MN (2010) The axon initial segment and the maintenance of neuronal polarity. Nat Rev Neurosci 11:552–562.
Saito K, Elce JS, Hamos JE, Nixon RA (1993) Widespread activation of calcium-activated neutral proteinase (calpain) in the brain in Alzheimer disease: a potential molecular basis for neuronal degeneration. Proc Natl Acad Sci USA 90:2628–2632.
Schafer DP, Jha S, Liu F, Akella T, McCullough LD, Rasband MN (2009) Disruption of the axon initial segment cytoskeleton is a new mechanism for neuronal injury. J Neurosci 29:13242–13254.
Sheehan JP, Swerdlow RH, Miller SW, Davis RE, Parks JK, Parker WD, Tuttle JB (1997) Calcium homeostasis and reactive oxygen species production in cells transformed by mitochondria from individuals with sporadic Alzheimer's disease. J Neurosci 17:4612–4622.
Sherriff F, Bridges L, Sivaloganathan S (1994) Early detection of axonal injury after human head trauma using immunocytochemistry for β-amyloid precursor protein. Acta Neuropathol 87:55–62.
Snowdon DA, Kemper SJ, Mortimer JA, Greiner LH, Wekstein DR, Markesbery WR (1996) Linguistic ability in early life and cognitive function and Alzheimer's disease in late life: findings from the Nun Study. JAMA 275:528–532.
Song A, Wang D, Chen G, Li Y, Luo J, Duan S, Poo M (2009) A selective filter for cytoplasmic transport at the axon initial segment. Cell 136:1148–1160.
Tanzi RE, et al. (1987) Amyloid beta protein gene: cDNA, mRNA distribution, and genetic linkage near the Alzheimer locus. Science 235:880–884.
Uhlen M, et al. (2015) Proteomics: tissue-based map of the human proteome. Science 347:1260419.
Wang B, Li H, Mutlu SA, Bowser DA, Moore MJ, Wang MC, Zheng H (2017) The amyloid precursor protein is a conserved receptor for slit to mediate axon guidance. eNeuro 4:ENEURO.0185-17.2017.
Whalley LJ, Starr JM, Athawes R, Hunter D, Pattie A, Deary IJ (2000) Childhood mental ability and dementia. Neurology 55:1455–1459.
White AR, et al. (1999) The Alzheimer's disease amyloid precursor protein modulates copper-induced toxicity and oxidative stress in primary neuronal cultures. J Neurosci 19:9170–9179.
Woods NK, Padmanabhan J (2012) Neuronal calcium signaling and Alzheimer's disease. Adv Exp Med Biol 740:1193–1217.
Xiao Q, et al. (2015) Neuronal-targeted TFEB accelerates lysosomal degradation of APP, reducing Abeta generation and amyloid plaque pathogenesis. J Neurosci 35:12137–12151.
Xu J, Ma H, Jin J, Uttam S, Fu R, Huang Y, Liu Y (2018) Super-resolution imaging of higher-order chromatin structures at different epigenomic states in single mammalian cells. Cell Rep 24:873–882.
Xu K, Zhong G, Zhuang X (2013) Actin, spectrin, and associated proteins form a periodic cytoskeletal structure in axons. Science 339:452–456.
Young-Pearse TL, Bai J, Chang R, Zheng JB, LoTurco JJ, Selkoe DJ (2007) A critical function for beta-amyloid precursor protein in neuronal migration revealed by in utero RNA interference. J Neurosci 27:14459–14469.
Zhang Y, et al. (2013) Rapid single-step induction of functional neurons from human pluripotent stem cells. Neuron 78:785–798.
Zhang Y, et al. (2014) An RNA-sequencing transcriptome and splicing database of glia, neurons, and vascular cells of the cerebral cortex. J Neurosci 34:11929–11947.
Zhang Y, et al. (2021) Fast and sensitive GCaMP calcium indicators for imaging neural populations. Biorxiv.
Zheng H, Koo EH (2006) The amyloid precursor protein: beyond amyloid. Mol Neurodegener 1:5.
Zhu B, Zhang Y, Herrup K (2019) Testing the neuroprotective properties of PCSO-524® using a neuronal cell cycle suppression assay. Mar Drugs 17:79.